



This is a repository copy of *Towards an Insight into the Dynamic Behaviour of Tray Distillation Columns Through Analysis and Simulation of Dynamically Asymmetric Packed Columns*.

White Rose Research Online URL for this paper:
<http://eprints.whiterose.ac.uk/75732/>

Monograph:

Nassehzadeh Tabrizi, M. H. (1979) *Towards an Insight into the Dynamic Behaviour of Tray Distillation Columns Through Analysis and Simulation of Dynamically Asymmetric Packed Columns*. Research Report. ACSE Research Report 113 . Department of Control Engineering, University of Sheffield

Reuse

Unless indicated otherwise, fulltext items are protected by copyright with all rights reserved. The copyright exception in section 29 of the Copyright, Designs and Patents Act 1988 allows the making of a single copy solely for the purpose of non-commercial research or private study within the limits of fair dealing. The publisher or other rights-holder may allow further reproduction and re-use of this version - refer to the White Rose Research Online record for this item. Where records identify the publisher as the copyright holder, users can verify any specific terms of use on the publisher's website.

Takedown

If you consider content in White Rose Research Online to be in breach of UK law, please notify us by emailing eprints@whiterose.ac.uk including the URL of the record and the reason for the withdrawal request.



eprints@whiterose.ac.uk
<https://eprints.whiterose.ac.uk/>

Am

629.8 (S)

TOWARDS AN INSIGHT INTO THE DYNAMIC BEHAVIOUR OF
TRAY DISTILLATION COLUMNS THROUGH ANALYSIS AND
SIMULATION OF DYNAMICALLY ASYMMETRIC PACKED COLUMNS.

by

M.H.NASSEHZADEH TABRIZI B.Sc., M.Sc.

Research Report No. 113

Department of Control Engineering,
University of Sheffield,
Mappin Street,
SHEFFIELD S1 3JD

October 1979

629.8 (S)

Am

7. List of symbols

α	- initial slope of equilibrium curve approximation
β	- relative volatility of mixture
c	- ratio of rectifier vapour-/stripper liquid capacitance
D	- molar distillate rate
F_l, F_v	- molar feed rates of liquid and vapour = F, where equal
G	- normalised spatial composition gradient in steady state
\underline{G}	- transfer function matrix (T.F.M.)
\underline{G}^*	- inverse T.F.M.
\underline{G}^*_{-A}	- inverse T.F.M. of multivariable first-order lag approximation
g_1^*, g_2^*	- diagonal elements of \underline{G}^*
g_{A1}^*, g_{A2}^*	- diagonal elements of \underline{C}^*_{-A}
$H_l, H_l' (=H_2)$	- liquid capacitances p.u. length of rectifier and stripper
$H_v (=H_1), H_v'$	- vapour capacitances p.u. length of rectifier and stripper
h'	- distance along column (measured from feed point in Section 1 and from ends from Section 2.2)
$\Delta h'$	- length of shell cell of column
h	- normalised distance ($h' k/V$)
$h_a(p), h_b(p)$	- transfer functions of accumulator and reboiler {= $h_e(p)$ where identical}
\underline{I}	- unit diagonal 2x2 matrix
k_r, k_s	- rectifier and stripper coefficients of cross-flow (evaporation) p.u. length (=k where identical)
\underline{K}	- controller gain matrix
k_1, k_2	- diagonal elements of \underline{K}
L_1', L_2'	- lengths of entire rectifier and stripper (=L' where identical)
L	- normalised value of L'
$L_r (=L), L_s, \ell$	- molar flows of liquid in rectifier and stripper and small changes therein
n	- cell number
p	- Laplace variable for transforms w.r.t. τ

5 066205 01



Towards an insight into the dynamic behaviour of tray distillation columns through analysis and simulation of dynamically asymmetric packed columns.

Summary

Partial differential equations with necessary boundary conditions are derived for the large and small signal behaviour of compositions in an ideal distillation column separating a binary mixture. The column considered is symmetrical in all respects (as in Edwards⁽¹⁾ and Guilandoust's⁽⁵⁾ earlier analyses and computations) but now includes unequal vapour and liquid capacitances.

This work involves the derivation of a completely analytical parametric (T.F.M.) in a more general form rather than the special case of equal vapour and liquid capacitances studied by Edwards. It is demonstrated how a detailed study into packed columns can be made to relate to the behaviour of tray columns.

Frequency and time simulations have been successfully programmed and have produced satisfactory and consistent results.

Multi-pass systems concepts are applied to the time simulations and investigations of stability phenomena undertaken.

Amendment to
Research Report
No. 113

Introduction

Parametric transfer functions for the symmetrical spatially continuous distillation columns obtained by Edwards⁽¹⁾ introduced negative gain at high frequency, and positive static gain with non-minimum-phase effects for relatively long columns*. It was proved however, that long tray type columns⁽²⁾ exhibit positive gains for both high and low frequency so non-minimum-phase effects do not occur. This is due to the fact that when the total vapour and liquid flow, $V + L^{**}$ is suddenly increased in a packed column, this causes weaker vapour and richer liquid to be initially moved towards the accumulator and reboiler ends of the column respectively resulting a transient reduction in the overall separations $Y - X^{\dagger}$, even if the final response is positive.

In tray columns this initial reduction in $Y - X^{\dagger}$ does not occur because of the continuous equilibrium between vapour and liquid in each tray. Having two separate capacitances in the vapour and liquid streams which are coupled by an interphase resistance, the non-minimum-phase effect occurs only in the packed columns. But in the tray columns such effects do not happen because there is no interphase resistance due to continuous equilibrium between vapour and liquid.

For simplicity and for constructing a model in a completely diagonal form (i.e. dyadic form), as the special case studied by Edwards⁽¹⁾, the vapour and liquid capacitances were taken to be the same making

$$C = \frac{H_1 \text{ (vapour capacitance)}}{H_2 \text{ (liquid capacitance)}} = 1$$

To investigate the behaviour of the dynamics of tray columns through a study packed columns, C must be variable, because in tray columns the vapour capacitances are very small compared to the liquid capacitances⁺.

* short packed columns however have -negative static gain.

+ or, if not negligible, the vapour capacitance may be scaled and lumped with the liquid capacitances due to the absence of inter-phase resistance.

** see list of symbols.

In the special case model it is impossible to demonstrate the behaviour of the system with unequal vapour and liquid capacitances ($c = 1$), so there is an important need to construct a model in a more general form where C can be variable. Unlike the special case constructing such model involves in many difficulties, but it enjoys the advantage of being a model of far wider application, where not only can it produce the same results as the special case, but it also gives more freedom to study the relations between the two types of column.

1. Large signal model

1.1 Vapour/liquid equilibrium

The compositions (mole fractions of the lighter component in the binary mixture) of the vapour and liquid in the rectifier section of the column are represented by X, Y and those in the stripper by X', Y' , then the equilibrium of vapour compositions $Y_e, (Y'_e)$ for a given liquid compositions $X, (X')$ will be

$$\beta = Y_e (1-X) / \{X(1-Y_e)\} \quad (1)$$

$$\beta = Y'_e (1-X') / \{X'(1-Y'_e)\}$$

where β is the relative volatility which is constant for an ideal mixture (i.e. obeying Dalton's and Rayoult's laws). Fig. 1, shows the equilibrium relationship (1), and straight line approximations for the stripper and rectifier, an important point is the symmetry of both true equilibrium and its linear approximation about -45° line.

The equations of the straight line segments are

$$Y'_e = \alpha X' \quad (2)$$

and

$$Y_e = X/\alpha + (\alpha-1)/\alpha$$

where

$$\beta > \alpha = 1 + \epsilon, \quad \epsilon > 0$$

1.2 Large signal partial differential equations

Fig. 2 illustrates the process and flow rates of the liquid and vapour through the system. The cross-flow taking place from

liquid to vapour streams is shown in Fig. 3. where a thin cell of thickness δh at a height $h' = m \delta h'$ is chosen. Choosing the m^{th} rectifier cell, material balances on the vapour and liquid streams for the light component give

$$H_v \delta h' d/dt Y(m) = V_r \{Y(m-1) - Y(m)\} + K_r \{Y_e(m) - Y(m)\} \delta h' \quad (3)$$

$$H_l \delta h' d/dt X(m) = L_r \{X(m+1) - X(m)\} - K_r \{Y_e(m) - Y(m)\} \delta h'$$

where K_r is a distant coefficient of cross flow, H_v and H_l are the vapour and liquid capacitances per unit length. Taking $\delta h'$ infinitesimal, therefore can obtain the following partial differential equations.

$$H_v \partial Y / \partial t + V_r \partial Y / \partial h' = K_r (Y_e - Y) \quad (4)$$

$$-H_l \alpha \partial Y_e / \partial t + L_r \alpha \partial Y_e / \partial h' = K_r (Y_e - Y)$$

and for the stripper ($h' < 0$) can write

$$-H_l' \partial X' / \partial t + L_s \partial X' / \partial h' = K_s (X' - X_e') \quad (5)$$

$$H_v' \alpha \partial X_e' / \partial t + \alpha V_s \partial X_e' / \partial h' = K_s (X' - X_e')$$

and

$$X_e' \approx Y' / \alpha \quad (6)$$

1.3 Condition for symmetry

$$\begin{aligned} V_r &= \alpha L_r \\ L_s &= \alpha V_s \\ K_s &= K_c = K \\ L_s &= V_r = V \\ H_v &= H_v' \alpha = H_1 \\ H_l' &= H_l \alpha = H_2 \end{aligned} \quad (7)$$

systems p.d.e's reduce to

$$H_1 \frac{\partial Y}{\partial t} + V \frac{\partial Y}{\partial h} = K(Y_e - Y) \quad (8)$$

$$-H_2 \frac{\partial Y_e}{\partial t} + V \frac{\partial Y_e}{\partial h} = K(Y_e - Y)$$

$$-H_2 \frac{\partial X^t}{\partial t} + V \frac{\partial X^t}{\partial h} = K(X^t - X_e^t)$$

$$H_1 \frac{\partial X^t}{\partial t} + V \frac{\partial X^t}{\partial h} = K(X^t - X_c^t)$$

1.4 Normalising the p.d.e's in time and space

Assuming normalised distance $h = h' K/V$ and space $\tau = tK/H_2$ the p.d.e's (8) will simplify to

$$c \frac{\partial Y}{\partial \tau} + \frac{\partial Y}{\partial h} = Y_e - Y$$

$$-\frac{\partial Y_e}{\partial \tau} + \frac{\partial Y_e}{\partial h} = Y_e - Y \quad (9)$$

$$-\frac{\partial X^t}{\partial \tau} + \frac{\partial X^t}{\partial h} = X^t - X_e^t$$

$$c \frac{\partial X^t}{\partial \tau} + \frac{\partial X^t}{\partial h} = X^t - X_e^t$$

where $c = H_1/H_2$ ⁽¹⁰⁾, which, unlike Edwards analysis will be retained as a freely adjustable system parameter throughout this investigation.

1.5 Terminal boundary conditions

1.5.1 Reboiler

If the reboiler liquid is in equilibrium with its vapour, at normalised distance L_2 below the feed where $h = -L_2$, can obtain

$$H_b \frac{dX_e^t(-L_2)}{dt} = L_s X^t(-L_2) - (V_s + W) Y^t(-L_2) \quad (11)$$

but $L_s = V_s + W$

eliminating $Y^t(-L_2)$ in terms of $X_e^t(-L_2)$

and using equation (6)

$$H_b \frac{dX'_e(-L_2)}{dt} = L_s \{X'(-L_2) - \alpha X'_e(-L_2)\} \quad (12)$$

where H_b is the capacitance of the reboiler.

1.5.2 Accumulator

Here liquid is condensed from vapour at composition $Y(L_1)$, where L_1 is normalised length of rectifier, and it is returned to the column at the flow rate of L_1 , so can write

$$H_a \frac{dX(L_1)}{dt} = V_r Y(L_1) - (L_r + D)X(L_1) \quad (13)$$

where D is the distillate rate and H_a is the capacitance. For a constant volume of the accumulator.

$$V_r = L_r + D$$

so

$$H_a \frac{dX(L_1)}{dt} = V_r \{Y(L_1) - X(L_1)\} \quad (14)$$

and eliminating $X(L_1)$ in terms of $Y_e(L_1)$ by using (2), can write

$$H_a \alpha \frac{dY_e(L_1)}{dt} = V_r [\alpha \{1 - Y_e(L_1)\} - \{1 - Y(L_1)\}] \quad (15)$$

1.6 Feed-point boundary conditions

Assuming a thin cell at the feed point, as this tends to zero, so the cross-flow from liquid to vapour and accumulations terms vanishes, so in general we can write

$$V_s Y^*(0) + F_v z = V_r Y(0) \quad (16)$$

$$L_r X(0) + F_l Z = L_s X^*(0)$$

where z, Z are the compositions of the feed vapour and liquid.

1.7 Steady state solutions of the symmetrical system

1.7.1 Feed conditions for symmetry

From special case equations (7) and from overall mass balance considerations can obtain

$$F_V = F_\ell = F \quad (17)$$

and from (17) and (2), (8), (13), (15) it follows that column must be run such that

$$D = W = F = \epsilon L_r \quad (18)$$

if the relations for the feed compositions is such that

$$z = 1 - Z \quad (19)$$

i.e. the feed co-ordinate lie on the -45° line which is shown in Fig. 1.

if the feed mixture is in the equilibrium such that

$$z = \alpha Z \quad (20)$$

so can obtain

$$Z = \frac{1}{(1 + \alpha)} \quad (21)$$

this proves that the feed boundary conditions are also symmetrical and now they can be expressed as

$$X'_e(0) + \{1 - Y(0)\} = 2/(\alpha + 1) \quad (22)$$

$$\{1 - Y'_e(0)\} + X'(0) = 2/(\alpha + 1) \quad (23)$$

1.7.2 Steady-state solutions

Ignoring all time derivatives solutions for the systems p.d.e' s (8) subject to the special case (12), (15), (19) and (23) and ignoring all time derivatives

then setting $Q(h) = 1 - Y(h)$

and $Q_e(h) = 1 - Y_e(h)$

so

$$\begin{aligned}dQ/dh &= Q_e - Q \\dQ_e/dh &= Q_e - Q \\dX'/dh &= X' - X'_e \\dX'_e/dh &= X' - X'_e\end{aligned}\tag{24}$$

if

$$L_1 = L_2 = L$$

subject to

$$\begin{aligned}Q(L) &= \alpha Q_e(L) \\X'(-L) &= \alpha X'_e(-L)\end{aligned}\tag{25}$$

$$\begin{aligned}X'_e(0) + Q(0) &= 2/(\alpha+1) \\Q_e(0) + X'(0) &= 2/(\alpha+1)\end{aligned}\tag{26}$$

so

$$\begin{aligned}dQ/dh &= dQ_e/dh \stackrel{\Delta}{=} -G \\dX'/dh &= dX'_e/dh \stackrel{\Delta}{=} G'\end{aligned}\tag{27}$$

where G is constant.

from (26) can write

$$Q(0) - Q_e(0) = X'(0) - X'_e(0)\tag{28}$$

and from (24) and (27), (28) it follows that

$$G = G'\tag{29}$$

so

$$\partial y/\partial h = \partial y_e/\partial h = \partial X'/\partial h = \partial X'_e/\partial h = G\tag{30}$$

because of the symmetry.

$$\begin{aligned}Q(h) &= X'(-h) \\Q_e(h) &= X'_e(-h) \\X'(-h) &= 1 - Y(h) \\X'_e(-h) &= 1 - Y_e(h)\end{aligned}\tag{31}$$

also

$$Y(h) = Y(0) + Gh \quad (32)$$

$$Y_e(h) = Y_e(0) + Gh$$

From (24) and (27)

$$G = Q - Q_e = Q(0) - Q_e(0) \quad (33)$$

and from (26) and (31)

$$2Q(0) = G + 2/(\alpha+1) \quad (34)$$

BY eliminating $Q(0)$ it will follow that

$$2Q_e(0) = -G + 2/(\alpha+1) \quad (35)$$

but

$$Q(L) = Q(0) - GL \quad (36)$$

$$Q_e(L) = Q_e(0) - GL$$

and from (25) we can get -

$$Q(0) - GL = \alpha Q_e(0) - \alpha GL$$

$$G\epsilon h = \alpha Q_e(0) - Q(0)$$

taking (34) and (35) and eliminating $Q_e(0)$ in between them will produce

$$G = 2\epsilon / \{(\alpha+1)(2\epsilon L + \alpha + 1)\} \quad (37)$$

substituting for G in (34) and (35) yields

$$Q(0) = 2(\alpha + \epsilon L) / \{(\alpha+1)(2\epsilon L + \alpha + 1)\} \quad (38)$$

$$Q_e(0) = 2(1 + \epsilon L) / \{(\alpha+1)(2\epsilon L + \alpha + 1)\} \quad (39)$$

and also

$$y(0) = 1 - 2(\alpha + \epsilon L) / \{(\alpha+1)(2 + \epsilon L + \alpha + 1)\}$$

$$y_e(0) = 1 - 2(1 + \epsilon L) / \{(\alpha+1)(2\epsilon L + \alpha + 1)\}$$

from (36) we can get

$$Q(L) = 2\alpha / \{(\alpha+1)(2\epsilon L + \alpha + 1)\} \quad (40)$$

$$Q_e(L) = 2 / \{(\alpha+1)(2\epsilon L + \alpha + 1)\} \quad (41)$$

$$Q - Q_e = 2\epsilon / \{(\alpha+1)(2\epsilon L + \alpha + 1)\} = G \quad (42)$$

equations (37) and (42) form the basis for the linear composition profiles of Fig. 4.

2. Small signal model

By implicit differentiations of the large signal P.d.e's (3) and (4) can obtain small signal P.d.e's for the system.

$$H_v \frac{\partial y}{\partial t} + V_r \frac{\partial y}{\partial h^1} + (\partial Y / \partial h^1)_v = K_r (y_e - y) \quad (43)$$

$$-H_\ell \alpha \frac{\partial y_e}{\partial t} + Lr \alpha \frac{\partial y_e}{\partial h^1} + (\partial Y_e / \partial h^1) \alpha \ell = K_r (y_e - y)$$

$$-H_\ell' \frac{\partial x'}{\partial t} + L_s \frac{\partial x'}{\partial h^1} + (\partial X' / \partial h^1) \ell = K_s (x' - x'_e) \quad (44)$$

$$H_v' \alpha \frac{\partial x'_e}{\partial t} + V_s \alpha \frac{\partial x'_e}{\partial h^1} + (\partial X'_e / \partial h^1) \alpha v = K_s (x' - x'_e)$$

small signal perturbations are represented by lower-case letters: and upper-case symbols are quasi-constants and, by considering the symmetrical steady-state solutions produces the simplified form

$$H_1 \frac{\partial y}{\partial t} + V \frac{\partial y}{\partial h^1} + K Gv/V = K(y_e - y)$$

$$-H_2 \frac{\partial y_e}{\partial t} + V \frac{\partial y_e}{\partial h^1} + K G\ell/V = K(y_e - y) \quad (45)$$

$$-H_2 \frac{\partial x'}{\partial t} + V \frac{\partial x'}{\partial h^1} + K G\ell/V = K(x' - x'_e)$$

$$H_1 \frac{\partial x_e}{\partial t} + V \frac{\partial x_e}{\partial h^1} + K G\alpha v/V = K(x' - x'_e)$$

$$\partial / \partial h^1 \equiv (K \partial / \partial h) / V$$

2.1 Normalised small signal P.d.e's

Normalising small signal P.d.e.s with respect to distance $h = h^1 K / V$ and time $\tau = (tk / H_2)$ the system simplifies to

$$C \frac{\partial y}{\partial \tau} + \frac{\partial y}{\partial h} + Gv/V = y_e - y$$

$$- \frac{\partial y_e}{\partial \tau} + \frac{\partial y_e}{\partial h} + \alpha Gl/V = y_e - y$$

$$- \frac{\partial x'}{\partial \tau} + \frac{\partial x'}{\partial h} + Gl/V = x' - x'_e$$

$$C \frac{\partial x'_e}{\partial \tau} + \frac{\partial x'_e}{\partial h} + \alpha Gv/V = x' - x'_e$$

where again $C = H1/H2$

2.3 Inverted U-tube model

Solution for the terminal perturbations are simplified by bending the process into an inverted U tube, as shown in Fig. 5. The origins of h, h' will be redefined at the reboiler end rather than at the feed.

This will effect the sign of spatial derivatives in the rectifier section.

The modified equations will become in the form as follows:

$$C \partial y / \partial \tau - \partial y / \partial h + Gv/V = y_e - y \quad (i)$$

$$- \partial y_e / \partial \tau - \partial y_e / \partial h + \alpha Gl/V = y_e - y \quad (ii)$$

$$- \partial x' / \partial \tau + \partial x' / \partial h + Gl/V = x' - x'_e \quad (iii)$$

$$C \partial x'_e / \partial \tau + \partial x'_e / \partial h + \alpha Gv/V = x' - x'_e \quad (iv)$$

(47)

taking Laplace transforms of (47) in P with respect to τ and in s with respect to h .

$$(1+cp-s)\tilde{y} - \tilde{y}_e + Gv/V_s + \tilde{y}(0) = 0 \quad (i)$$

$$-(1+p+s)\tilde{y}_e + \tilde{y}_e + Gl/V_s + \tilde{Y}_e(0) = 0 \quad (ii)$$

$$-(1+p-s)\tilde{x}' + \tilde{x}' + Gl/V_s - \tilde{x}'(0) = 0 \quad (iii)$$

$$(1+cp+s)\tilde{x}'_e - \tilde{x}'_e + \alpha Gv/V_s - \tilde{x}'_e(0) = 0 \quad (iv)$$

(48)

where subscript \approx denotes transforms w.r.t.h, τ , and \sim w.r.t. τ only.

2.4. Matrix representation of the system

Matrix representation which will lead to the solution for the terminal composition variations. If input and output vectors are defined as

$$q = \begin{bmatrix} y-x' \\ y+x' \end{bmatrix}, \quad \Gamma = \begin{bmatrix} y_e - x'_e \\ y_e + x'_e \end{bmatrix}, \quad \underline{u} = \frac{G}{V} \begin{bmatrix} v+l \\ v-l \end{bmatrix} \quad (49)$$

2.4.1 Terminal boundary conditions

By implicit differentiation of the general large signal boundary conditions (12), (14) can achieve small perturbations as follows:-

$$H_a \alpha \, dy_e(0)/dt = V_r \{y(0) - \alpha y_e(0)\}$$

$$H_b \, dx'_e(0)/dt = L_s \{x'(0) - \alpha x'_e(0)\}$$

replacing the normalised time $\tau = tK/H_2$ and $V_r = L_s = V$ for the symmetry then

$$H_a \alpha \, k/H_2 V (dy_e(0)/d\tau) = y(0) - \alpha y_e(0) \quad (50)$$

$$H_b \, K/H_2 V (dx'_e(0)/d\tau) = x'(0) - \alpha x'_e(0)$$

Laplace transforming in P, will give

$$\tilde{Y}_e(0) = \alpha^{-1} h_a(P) \tilde{y}(0) \quad (51)$$

$$\tilde{x}'_e(0) = \alpha^{-1} h_b(P) \tilde{x}'(0)$$

where

$$h_a(P) = 1/(1+T_a P)$$

$$h_b(P) = 1/(1+T_b P)$$

and

$$T_a = H_a k / H_2 V \quad (52)$$

$$T_b = H_b k / H_2 V \alpha$$

again assuming the symmetry

$$h_a(p) = h_b(p) \triangleq h_e(p)$$

from (49) and (50)

$$\tilde{r}(0) = \alpha^{-1} h_e(p) \tilde{q}(0) \quad (53)$$

2.4.2 Feed boundary conditions

By implicit differentiation of large-signal (16) boundary conditions for constant flows and compositions.

$$V_s y'(0) - V_r y(0) + \{Y'(0) - Y(0)\} v = 0$$

$$L_r x(0) - L_s x'(0) + \{X(0) - X'(0)\} \ell = 0$$

substituting $x(0)$, $y'(0)$ by $\alpha y_e(0)$ and $\alpha x'_e(0)$ and substituting steady state flow conditions for symmetry yields

$$x'_e(0) - y(0) - \{Y(0) - Y'(0)\} v/V = 0$$

$$y_e(0) - x'(0) + \{X(0) - X'(0)\} \ell/V = 0$$

and using steady state solutions (30), (37)

$$y(0) = x'_e(0) - (\epsilon/2) Gv/V$$

$$x'(0) = y_e(0) + (\epsilon/2) G\ell/V$$

putting these equations back in inverted U tube form will give

$$y(L) = x'(L) - (\epsilon/2) Gv/V \quad (54)$$

$$x'(L) = y_e(L) + (\epsilon/2) G\ell/V$$

Adding and subtracting equation (54) will produce

$$q(L) = \begin{pmatrix} -1 & 0 \\ 0 & 1 \end{pmatrix} \underline{r}(L) - (\epsilon/2) \underline{u} \quad (55)$$

2.4.3 Solutions

Adding and subtracting pairs of equations (48) will produce simple equations.

from (i) and (ii)

$$(1-s)\underline{\tilde{q}} + cp\begin{pmatrix} 1 \\ 1 \end{pmatrix}\underline{\tilde{y}} + p\begin{pmatrix} -1 \\ 1 \end{pmatrix}x' - \underline{\tilde{r}} = -s^{-1}\underline{\tilde{u}} - \underline{\tilde{q}}(0) \quad (56)$$

but from (49)

$$q_1 = y - x'$$

and $q_2 = y + x'$

$$q_1 - q_2 = -2x'$$

$$\underline{\tilde{x}}' = \frac{q_2 - q_1}{2} \quad (57)$$

$$q_1 + q_2 = 2y, \quad \underline{\tilde{y}} = \frac{q_1 + q_2}{2} \quad (58)$$

Using equations (56) and (58)

$$cp \begin{pmatrix} 1 \\ 1 \end{pmatrix} \underline{\tilde{y}} = \frac{cp}{2} \begin{pmatrix} 1 \\ 1 \end{pmatrix} (1 \ 1) \underline{\tilde{q}} = cp/2 \begin{pmatrix} 1 & 1 \\ 1 & 1 \end{pmatrix} \underline{\tilde{q}}$$

and also from (56) and (57)

$$p\begin{pmatrix} -1 \\ 1 \end{pmatrix} \underline{\tilde{x}}' = p/2\begin{pmatrix} -1 \\ 1 \end{pmatrix} (-1 \ 1) \underline{\tilde{q}} = p/2\begin{pmatrix} 1 & -1 \\ -1 & 1 \end{pmatrix} \underline{\tilde{q}}$$

substituting back into (49)

$$\{(1-s)I + p/2 \begin{pmatrix} c+1 & c-1 \\ c-1 & c+1 \end{pmatrix}\} \underline{\tilde{q}} - \underline{\tilde{r}} = -s^{-1}\underline{\tilde{u}} - \underline{\tilde{q}}(0) \quad (59)$$

from (iii) and (v) in (48)

$$-(1+s)\underline{\underline{r}} + p\begin{pmatrix} -1 \\ -1 \end{pmatrix}\underline{\underline{y}}_e + cp\begin{pmatrix} 1 \\ -1 \end{pmatrix}\underline{\underline{x}}'_e + q = \alpha s^{-1}\begin{pmatrix} -1 & 0 \\ 0 & 1 \end{pmatrix}\underline{\underline{u}} - \underline{\underline{r}}(0) \quad (60)$$

using (49)

$$\underline{\underline{y}}_e = \frac{r_1 + r_2}{2}$$

$$\underline{\underline{x}}'_e = \frac{r_2 - r_1}{2}$$

$$p\begin{pmatrix} -1 \\ -1 \end{pmatrix}\underline{\underline{y}}_e = p/2 \begin{pmatrix} -1 \\ -1 \end{pmatrix}(1 \quad 1)\underline{\underline{r}} = -p/2\begin{pmatrix} 1 & 1 \\ 1 & 1 \end{pmatrix}\underline{\underline{r}}$$

$$cp\begin{pmatrix} 1 \\ -1 \end{pmatrix}\underline{\underline{x}}'_e = cp/2\begin{pmatrix} 1 \\ -1 \end{pmatrix}(-1 \quad 1)\underline{\underline{r}} = -cp/2\begin{pmatrix} 1 & -1 \\ -1 & 1 \end{pmatrix}$$

substituting into (60)

$$-\{(1+s)I + p/2\begin{pmatrix} 1+c & 1-c \\ 1-c & 1+c \end{pmatrix}\}\underline{\underline{r}} + \underline{\underline{q}} = \alpha s^{-1}\begin{pmatrix} -1 & 0 \\ 0 & 1 \end{pmatrix}\underline{\underline{u}} - \underline{\underline{r}}(0) \quad (61)$$

from (59)

$$r = \{(1-s)I + p/2\begin{pmatrix} c+1 & c-1 \\ c-1 & c+1 \end{pmatrix}\}\underline{\underline{q}} + s^{-1}\underline{\underline{u}} + \underline{\underline{q}}(0) \quad (62)$$

substituting (62) into (61)

$$- \begin{bmatrix} 1+s+p/2+cp/2 & p/2-cp/2 \\ p/2 - cp/2 & 1+s+p/2+cp/2 \end{bmatrix} \begin{bmatrix} 1-s+p/2+cp/2 & cp/2-p/2 \\ cp/2-p/2 & 1-s+cp/2+p/2 \end{bmatrix} \underline{\underline{q}}$$

$$- \begin{bmatrix} 1+s+p/2+cp/2 & p/2-cp/2 \\ p/2-cp/2 & 1+s+p/2+cp/2 \end{bmatrix} s^{-1}\underline{\underline{u}} -$$

(63)

$$\begin{bmatrix} 1+s+p/2+cp/2 & p/2-cp/2 \\ p/2-cp/2 & 1+s+p/2+cp/2 \end{bmatrix} \underline{\underline{q}}(0) + \underline{\underline{q}} = \\ = \alpha s^{-1}\begin{pmatrix} -1 & 0 \\ 0 & 1 \end{pmatrix} \underline{\underline{u}} - \underline{\underline{r}}(0)$$

using (53) in (63) yields

$$\begin{bmatrix} s^2 - cp^2 - cp - p & sp - scp \\ sp - scp & s^2 - cp^2 - cp - p \end{bmatrix} \underline{\underline{q}} =$$

$$s^{-1} \begin{bmatrix} 1+s+p/2+cp/2-\alpha & p/2-cp/2 \\ p/2-cp/2 & 1+s+p/2+cp/2+\alpha \end{bmatrix} \underline{\underline{u}} +$$

$$\begin{bmatrix} 1+s+p/2+cp/2-\alpha^{-1}h & p/2-cp/2 \\ p/2-cp/2 & 1+s+p/2+cp/2-\alpha^{-1}h \end{bmatrix} \underline{\underline{q}}(0) \quad (64)$$

From (64)

$$\underline{\underline{q}} = H \begin{bmatrix} s^2 - cp^2 - cp - p & scp - sp \\ scp - sp & s^2 - cp^2 - cp - p \end{bmatrix} *$$

$$s^{-1} \begin{bmatrix} 1+s+p/2+cp/2-\alpha & p/2-cp/2 \\ p/2-cp/2 & 1+s+p/2+cp/2+\alpha \end{bmatrix} \underline{\underline{u}} +$$

$$\begin{bmatrix} 1+s+p/2+cp/2-\alpha^{-1}h & p/2-cp/2 \\ p/2-cp/2 & 1+s+p/2+cp/2-\alpha^{-1}h \end{bmatrix} \underline{\underline{q}}(0) \quad (65)$$

where $H = \frac{1}{(s^2 - cp^2 - cp - p)^2 - (sp - scp)^2}$

substituting (65) in (62) will give

$$\underline{\underline{r}} = H \begin{bmatrix} s^2 - cp^2 - cp - p & scp - sp \\ scp - sp & s^2 - cp^2 - cp - p \end{bmatrix} *$$

$$s^{-1} \begin{bmatrix} 1-\alpha(1+p/2+cp/2)+\alpha s & \alpha cp/2 - p/2 \\ -\alpha cp/2 + \alpha p/2 & 1+(1+p/2+sp/2)\alpha - \alpha s \end{bmatrix} \underline{\underline{u}} +$$

$$\begin{bmatrix} 1-(1+p/2+cp/2)\alpha^{-1}h + s\alpha^{-1}h & -(cp/2-p/2)\alpha^{-1}h \\ -(cp/2-p/2)\alpha^{-1}h & 1-(1+p/2+cp/2)\alpha^{-1}h + s\alpha^{-1}h \end{bmatrix} \underline{\underline{q}}(0) \quad (66)$$

substituting (65) and (66) in (65) can achieve the solutions for $q_{1,2}$. Because of the complicated nature of the resulting expressions, this operation is best left to the computer. (In Edwards study, the simplicity of the completely symmetrical system allowed substitutions to be carried out analytically). The symmetric systems T.F.M. could be obtained completely analytically but the complexity of the resulting expressions would make them of little practical use.

3. Time simulation

Two methods to simulate the systems equations based on multipass process analysis are applied. There was a difficulty in simulating the system because of the feed at the middle of distillation column and the complicated boundary conditions. But by trying to keep the system as simple as possible results were satisfactorily obtained. First attempt was made to simulate the systems equations (47) in U tube form where tube was bent from the middle and also the four equations were transformed to two by combining (i) and (iii), (ii) and (iv), resulting for the special case $C = 1$.

$$\frac{\partial y}{\partial \tau} - \frac{\partial y}{\partial h} + G/v = y_e - y \quad (i)$$

$$- \frac{\partial y_e}{\partial \tau} - \frac{\partial y_e}{\partial h} + \alpha G l/v = y_e - y \quad (ii)$$

$$- \frac{\partial x'}{\partial \tau} + \frac{\partial x'}{\partial h} + G l/v = x' - x'_e \quad (iii)$$

$$\frac{\partial x'_e}{\partial \tau} + \frac{\partial x'_e}{\partial h} + \alpha G l/v = x' - x'_e \quad (v)$$

adding (i) and (iii) gives

$$\frac{\partial (y-x')}{\partial \tau} - \frac{\partial (y-x')}{\partial h} + \frac{G}{v} (v+l) = (y_e - x'_e) - (y-x')$$

and from (ii) and (v)

$$- \frac{\partial (y_e - x'_e)}{\partial \tau} - \frac{\partial (y_e - x'_e)}{\partial h} + \frac{\alpha G}{v} (v+l) = (y_e - x'_e) - (y-x')$$

This method has produced more accurate results*, because there are half the number of equations involved in the simulation i.e. reducing the number of round-off errors. Again this method is only for the special case where $C = 1$ and disadvantages of this have already been discussed. For the more general

* The boundary conditions can be produced from (50), (54) in the same way.

Time responses of the U tube model are shown in Figures 16, 17.

case, the straight tube approach, sweeping up from the reboiler to the accumulator and back (involving a switch of equations at the feed point), was formed to generate more reliable solution. It has been noticed that by having only one multipass loop (i.e. as for the straight tube model), makes the simulation easier as well as producing satisfactory and stable results. Fig.3.1 explains more about the simulation. Equations(46) have been simulated as the straight tube and the multipass process analysis has been applied to the two different methods of numerical solution.

3.1 Analysis of methods of simulations by multipass system theory

Packed column and heat exchanger p.d.e's take the form

$$\frac{\partial \phi_1}{\partial \tau} = - \frac{\partial \phi_1}{\partial h} - \phi_1 + \phi_2 + U_1$$

$$\frac{\partial \phi_2}{\partial \tau} = \frac{\partial \phi_2}{\partial h} + \phi_1 - \phi_2 + U_2$$

where τ = normalised time. and h = normalised distance.

Numerical scheme

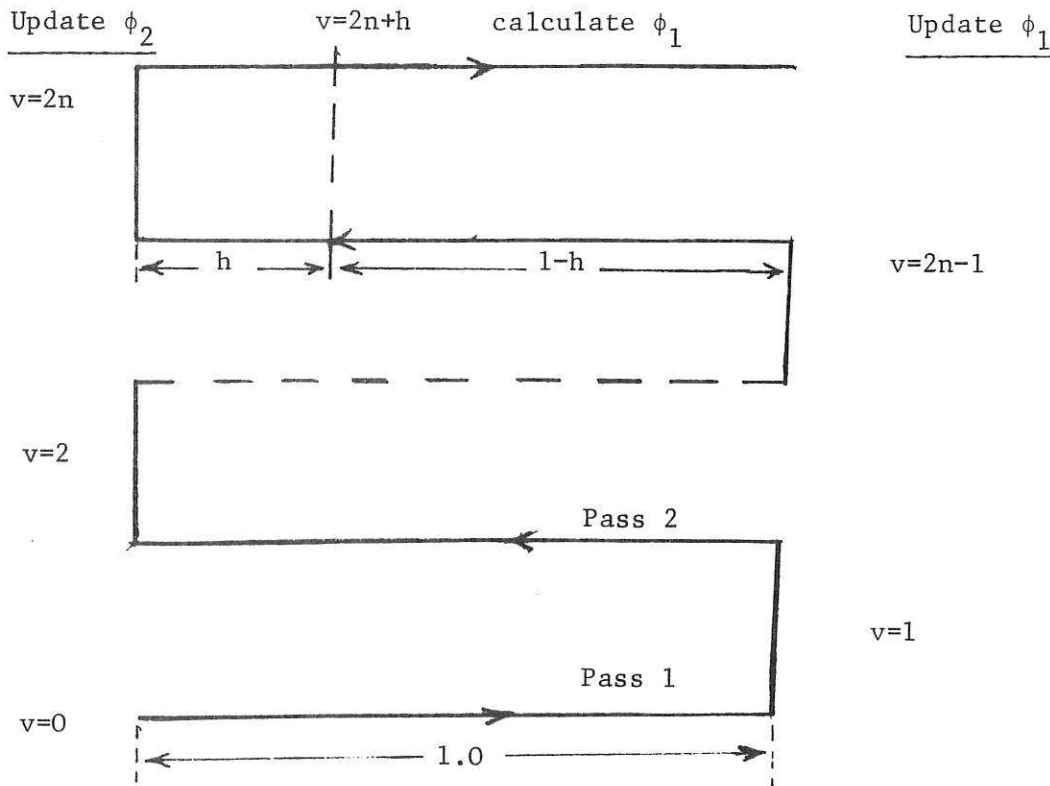


Figure 3.1

Two different methods of updating which are discussed later, were applied and they both produced the satisfactory results. The methods are different from one another as regards their stability criteria:

3.1.1 Simulation and stability criteria

3.1.1.1 Method 1, Immediate updating

$$\frac{\phi_1(\tau) - \phi_1(\tau - T)}{\Delta T} = \text{approximate time derivative where } \Delta T = \text{complete process update interval.}$$

To a distance base, $\phi_1(\tau) = \phi_1(v)$ and distance increment is covered in interval

$$\Delta T = 2 \text{ process lengths} = 2$$

so
$$\frac{\partial \phi_1(h, \tau)}{\partial \tau} = \frac{\phi_1(v) - \phi_1(v-2)}{\Delta T}$$

$$\phi_1(h, \tau) = \phi_1(v)$$

$$\frac{\partial \phi_1(h, \tau)}{\partial h} = \frac{\phi_1(v) - \phi_1(v - \delta h)}{\delta h}$$

but $\phi_2(h, \tau)$ must be approximated by

$$\phi_2(v-2h), \text{ where } 2m < v < 2m+1, m=0,1,\dots$$

during left hand sweeps $2m+1 < v < 2m+2, m=0,1,\dots$

$$\frac{\partial \phi_2(h, \tau)}{\partial \tau} = \frac{\phi_2(v) - \phi_2(v-2)}{\Delta T}$$

$$\phi_2(h, \tau) = \phi_2(v)$$

$$\frac{\partial \phi_2(h, \tau)}{\partial h} = -\frac{\phi_2(v) - \phi_2(v - \delta h)}{\delta h}$$

but $\phi_1(h, \tau)$ must be approximated by

$$\phi_1\{v-2(1-h)\}.$$

substituting these approximations we obtain

$$\frac{\phi_1(v) - \phi_1(v-2)}{\Delta T} = \frac{\phi_1(v-\delta h) - \phi_1(v)}{\delta h} - \phi_1(v) + \phi_2(v-2h) + U_1(v)$$

$$\frac{\phi_2(v) - \phi_2(v-2)}{\Delta T} = \frac{\phi_2(v-\delta h) - \phi_2(v)}{\delta h} + \phi_1\{v-2(1-h)\} - \phi_2(v) + U_2(v)$$

$$\tilde{\phi}_1 \left\{ \frac{1}{\Delta T} - \frac{e^{-2s}}{\Delta T} - \frac{e^{-\delta h s}}{\delta h} + \frac{1}{\delta h} + 1 \right\} = \tilde{\phi}_2 e^{-2hs} + \tilde{U}_1$$

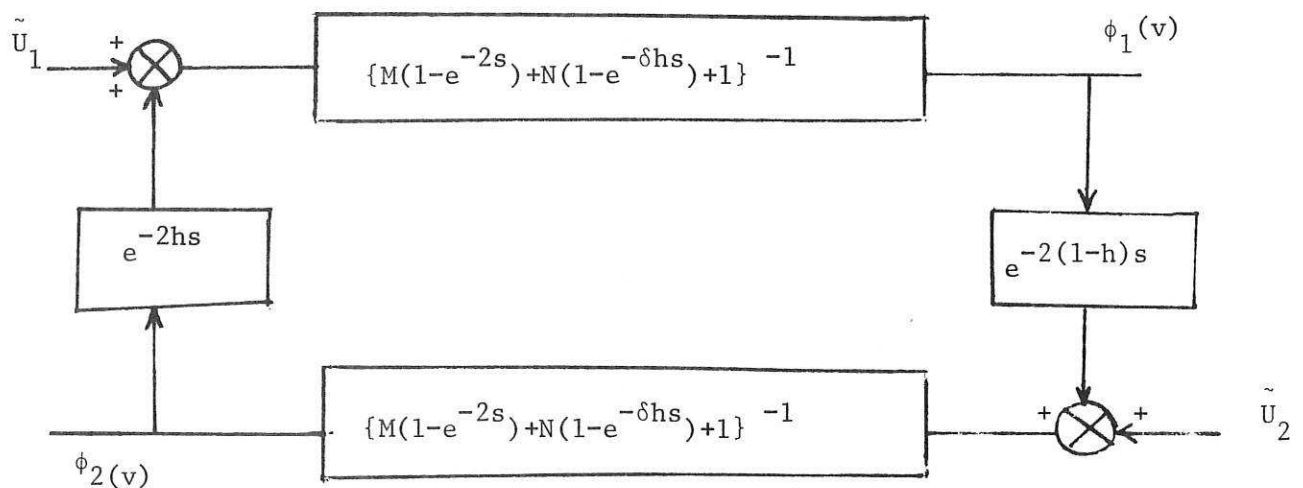
$$\tilde{\phi}_2 \left\{ \frac{1}{\Delta T} - \frac{e^{-2s}}{\Delta T} - \frac{e^{-\delta h s}}{\delta h} + \frac{1}{\delta h} + 1 \right\} = \tilde{\phi}_1 e^{-2(1-h)s} + \tilde{U}_2$$

Now if there are N special cells, $\delta h = N^{-1}, \Delta T = M^{-1}$

$$\therefore \tilde{\phi}_1 \{M(1-e^{-2s}) + N(1-e^{-\delta h s}) + 1\} = \tilde{\phi}_2 e^{-2hs} + \tilde{U}_1$$

$$\tilde{\phi}_1 \{M(1-e^{-2s}) + N(1-e^{-\delta h s}) + 1\} = \tilde{\phi}_1 e^{-2(1-h)s} + \tilde{U}_2$$

yielding the block diagram



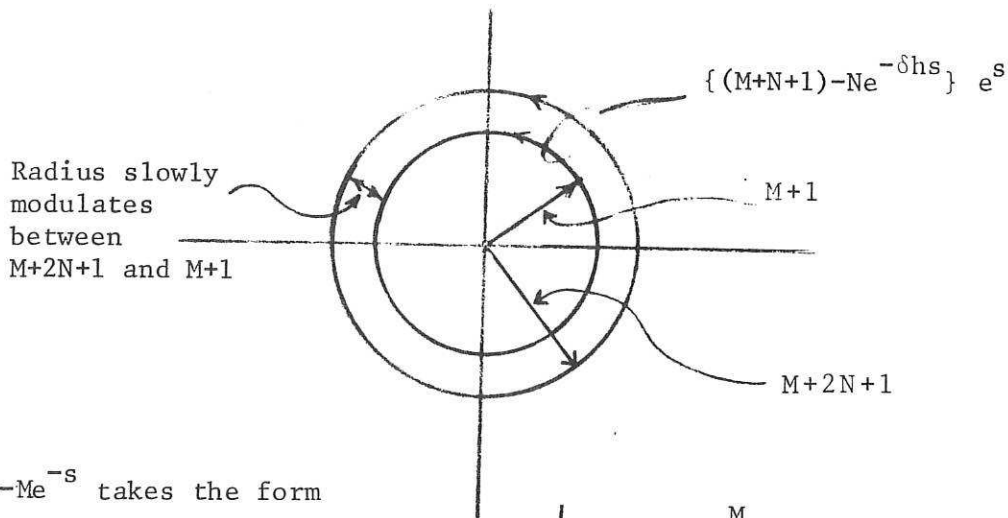
The open-loop T.F. is therefore:

$$\begin{aligned}
 & -\{M(1-e^{-2s})+N(1-e^{-\delta hs})+1\}^2 e^{2s} \\
 = & -\{M(e^s-e^{-s})+N(e^s-e^{(1-\delta h)s})+e^s\}^2 \\
 = & -\{(M+N+1)e^s-Me^{-s}-Ne^{(1-\delta h)s}\}^2
 \end{aligned}$$

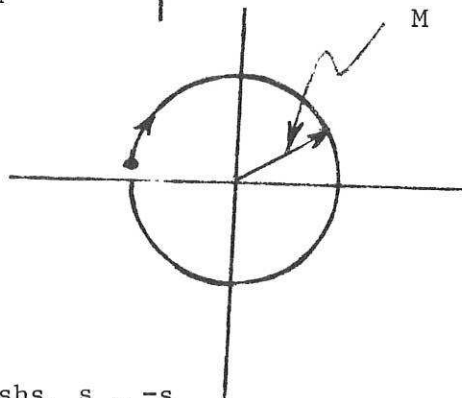
or $-\{(M+N+1-Ne^{-\delta hs})e^s-Me^{-s}\}^2$

consider $(M+N+1-Ne^{-\delta hs})e^s$

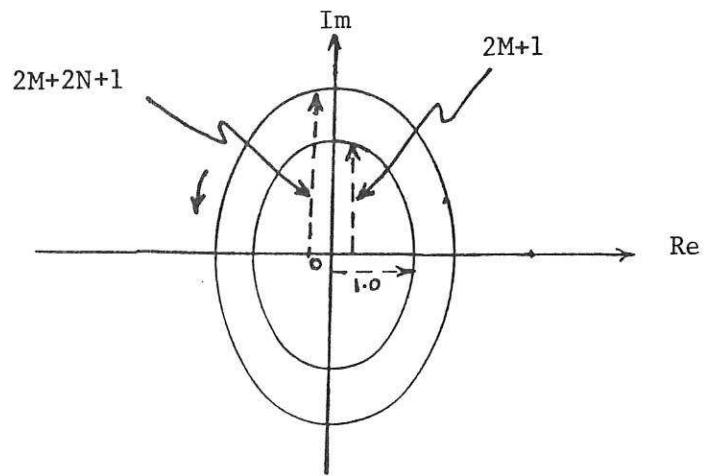
since $M+N+1 > N$ the locus for $s = j\omega$ will take the form



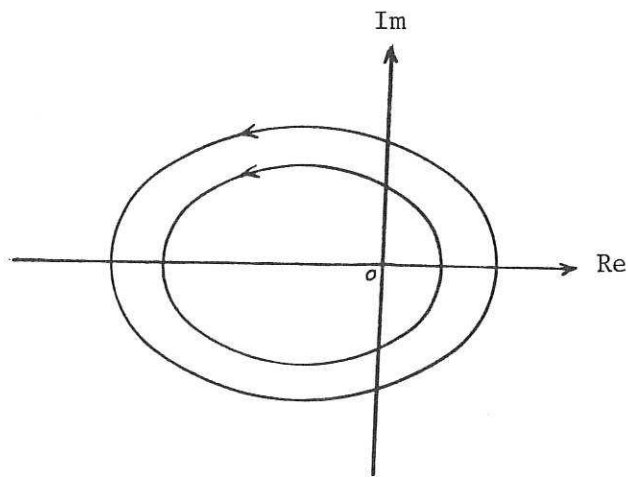
$-Me^{-s}$ takes the form



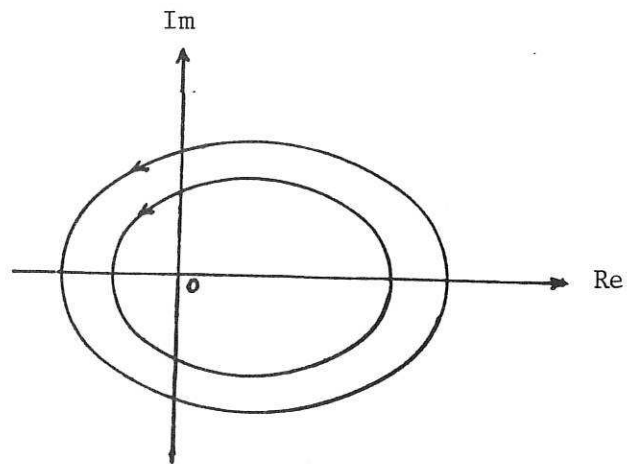
resultant $(M+N+1-Ne^{-\delta hs})e^s-Me^{-s}$



squaring



negating



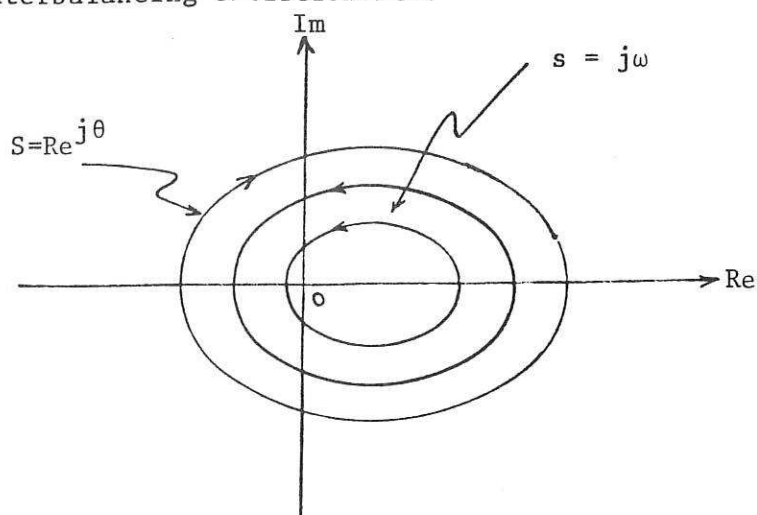
$$s = R_e j^\theta$$

O.L.T.F.

$$(M+N+1) e^{R_e j^\theta}$$

since $R_e(s) > 0$ for $-\pi/2 < \theta < \pi/2$

therefore as θ falls from $\pi/2$ to $-\pi/2$ so O.L.T.f. locus also rotates clockwise yielding counterbalancing encirclements.



open loop system should be stable (end effects neglected).

3.1.1.2 Method 2, updating at the end of sweep

set $\phi_1(h, \tau) = \phi_1(v-2)$

$$\frac{\partial \phi_1(h, \tau)}{\partial h} = \frac{\phi_1(v-2) - \phi_1(v-2 - \delta h)}{\delta h}$$

similarly with ϕ_2 & $\frac{\partial \phi_2}{\partial h}$ so

$$\frac{\phi_1(v) - \phi_1(v-2)}{\Delta T} = \frac{\phi_1(v-2 - \delta h) - \phi_1(v-2)}{\delta h} - \phi_1(v-2) + \phi_2(v-2h) + U_1(v)$$

$$\frac{\phi_2(v) - \phi_2(v-2)}{\Delta T} = \frac{\phi_2(v-2 - \delta h) - \phi_2(v-2)}{\delta h} + \phi_1\{v-2(1-h)\} + \phi_2(v-2) + U_2(v)$$

therefore $\tilde{\phi}_1 \left\{ \frac{1-e^{-2s}}{\Delta T} + e^{-2s} \frac{(1-e^{-\delta h s})}{\delta h} + e^{-2s} \right\} = \tilde{\phi}_2 e^{-2hs} + \tilde{U}_1$

$$\phi_2 \left\{ \frac{1-e^{-2s}}{\Delta T} + e^{-2s} \frac{(1-e^{-\delta h s})}{\delta h} + e^{-2s} \right\} = \tilde{\phi}_2 e^{-2(1-h)s} + \tilde{U}_2$$

if $\delta h = N^{-1}$, $\Delta T = M^{-1}$

$$\tilde{\phi}_1 \{M(1-e^{-2s}) + Ne^{-2s}(1-e^{-\delta hs}) + e^{-2s}\} = \tilde{\phi}_2 e^{-2hs} + \tilde{U}_1$$

$$\tilde{\phi}_2 \{M(1-e^{-2s}) + Ne^{-2s}(1-e^{-\delta hs}) + e^{-2s}\} = \hat{\phi}_1 e^{-2(1-h)s} + \hat{U}_2$$

therefore in this case inverse O.L.T.F. =

$$-\{M(1-e^{-2s}) + Ne^{-2s}(1-e^{-\delta hs}) + e^{-2s}\} e^{2s}$$

$$= -\{M(e^s - e^{-s}) + Ne^{-s} - Ne^{-(1+\delta h)s} + e^{-s}\}^2$$

$$= -\{Me^s - e^{-s}(M-1-N+Ne^{-\delta hs})\}^2$$

for stability $|e^s|$ term must dominate $|e^{-s}|$ term

$$s = jw$$

$$M > M-1, \quad M > 2N+1$$

$$\text{and } M > |M-1-2N| \quad M > 2N+1$$

$$\text{i.e. } M > 2N+1-M, \quad 2N+1 > M$$

therefore $2M > 2N+1, \quad M < 2N+1$

$$\text{and } \frac{2N+1}{2} < M$$

i.e. time step < distance step

Hence provided the above condition is satisfied the simulation should be stable - end effects neglected.

Note Multi-pass analysis does not embrace end effects and these may cause instability despite the predictions of multi-pass theory. This point is brought out in the following section.

Typical graphs for both methods of updating the multi pass system theory are given in Fig. 8, 10 and Fig. 15 shows the stability phenomena for both methods.

Notes on the results

Both special case and general case methods have been simulated by the author,

and have produced satisfactory and consistent results

obtained for systems having parameters identical in many cases, to those used in this earlier work. The complete agreement for the symmetrical case of these earlier results with those derived and computed completely independently by the present author gives confidence in the general assymmetric system results presented here and never previously obtained.

For given parameters the time and frequency responses have produced the same steady state gain and equal time constants as is demonstrated below.

q_1 represents the first element of the composition vectors, and

$$\tilde{q}(h,p) = \underline{G}(h,p) \tilde{U}(p)$$

$$\text{and } \tilde{U}(p) = \underline{G}^*(h,p) * \tilde{q}(h,p)$$

$$\underline{G}^*(h,p) = \begin{vmatrix} g_1^*(h,p) & g_2^*(h,p) \\ g_3^*(h,p) & g_4^*(h,p) \end{vmatrix}$$

$$\underline{G}^*(h,p) = 1/\underline{G}(h,p)$$

All of the responses have been explained individually as they follow:

Fig. 6. Represents behaviours of special⁺ and general case⁺ models for the given parameters. By taking $C = 1$ both models produce exactly the same results and this validates the general case model. Frequency range is chosen to be the same for both cases. Loops due to travelling wave effects are clearly visible, as would be expected for a comparatively short columns such as this (note $L = 2.8$)

Fig. 7. Inverse Nyquist Loci for the short columns with its m.v. first order lag³ approximations constant frequency increments are marked on the Loci and they almost match with those on the m.v. first order lag approximations. Also it is shown on the inverse Nyquist Loci that the number of frequency increments on each loop are nearly equal to one another and = theoretically, $L=2.8$ as would be expected, these demonstrates the validity of the m.v. first order lag and the better lag delay approximations as well as giving

To find the time constant consider the T.f. for the first order lag

$$G(j\omega) = \frac{K}{1+j\omega T}$$

$$\tan^{-1} \omega T = 45$$

$$\omega T = 1$$

$$T = \frac{1}{\omega}$$

by drawing a 45° line with axis can find the frequency corresponding to the point where the 45° line crosses the inverse nyquist loci, and so can find the time constant from the graph, the frequency is found to be 2, so $T = \frac{1}{2} = 0.5$, the steady state value is simply the value of $g_1(0,0)$ and from the graph $g_1^{-1}(0,0) = 1.8$ and $g_1(0,0) = 0.55$. These values compare favourably with those step responses of Fig. 9.

Fig. 8. Time response of the short column parameters are chosen to be the same as for Fig. 7. Two different methods of updating used to simulate the system by the multi-pass approach are shown to have the same initial rate of rise and equal steady state values.

Time constant $\underline{\Delta}$ 0.6

Steady state gain = 0.46

clearly these values almost agree with those of Fig. 7.

Fig. 9. Inverse Nyquist loci for a longer column $L=5.0$ with a m.v. first order lag approximation. It is shown that the static gain $g_1(0,0)$ is positive whereas over higher frequency range the gain is negative, so m.v. first order lag approximations is not valid.

(Due to the different signs of elements of matrices $\underline{A1}$ and $\underline{A0}$): the locus of the m.v. lag clearly does not encircle the origin as does the true locus.

Time constant = 10

$g_1(0,0) = 1.43$

again these values will be compared with those on Fig. 10.

Note smaller loops due to wave attenuations in longer columns.

Fig. 10. Time responses of the long column, with parameters same as for Fig. 9. Two different methods of updating used to simulate the system by the multi-pass approach are shown to be the same.

Time constant = 10

steady state gain = 1.45

these values are similar with those on Fig. 9.

Figs 11,12 Represents $g_1^{-1}(0, j\omega)$ with different end capacitances. Large end capacitance would appear to effect only the frequency calibration of the loci near $\omega = 0$, rather than their basic shape, this is clear from the graph and would be expected since it is known that boundary conditions affect predominantly steady state behaviour and not the high frequency.

Fig. 13 Time responses of the long columns with different end capacitances, from the graphs it is clear that the initial rate of rise and the steady state value for both responses are the same.

Fig. 14 Time responses of the short columns with different end capacitances.

Fig. 15 Time responses of the short column. This graph represents responses achieved from the two different methods of updating. It is shown how one method can go unstable while the other is still stable - as anticipated.

Figs 16,17 Time response of the short column obtained from the inverted U tube model.

Fig. 18 Inverse Nyquist loci of plate column, response shows that the model behaves as first order lag, and non-minimum phase effects are none existant. The frequency calibration is clearly almost linear with vertical distance measured along the locus ,

and this validates the m.v. first order approximations for this model.

Fig. 19 Time response of the plate column. Again the response shows the system behaves as a first order lag, and the close agreement of the steady state gain (2.6) with that shown in Fig. 18 ($1/0.37 = 2.7$) is reassuring.

5. Relating the dynamic behaviour of the packed and plate columns and effect changing L and C.

Differences between the behaviour of packed and plate columns left some questions to be answered and whether packed columns analysis is useful in industry, where columns are predominantly of the plate type. In particular the non-minimum phase effects of packed columns noted in section (4) Figs.9, 10, are not produced by tray columns. However in this section it is shown by time domain simulation and by frequency response analysis that as the length L is increased and as the liquid/vapour capacitance ratio is increased (for a given total capacitance) so the non-minimum phase effect diminishes to negligible proportions and the dynamic response match more and more closely. Under these circumstances therefore the packed column approach can provide a useful alternative to the modelling of industrial tray type columns.

As regards the effect of column length relation noted in section (2.1) confirm this observation: since $h = h'K/V$ and in particular $L = L'K/V$ it is clear that as $L \rightarrow \infty$, so $K \rightarrow \infty$, for a given real length L. So increase in L is equivalent to an increase in evaporations constant K, an increase of which clearly approaches the continuous equilibrium condition assumed in tray column models.

In order to relate the behaviour of the two columns together, an attempt was made to make responses of two columns to settle at the same steady state response values for given different parameters for each column. This was done by equating Edwards' analytically derived relation for zero frequency gain^{1,2}, for both columns of equal length. Although this produced quite satisfactory results as comparison of Figs. 10 and 20(a) of time responses and also comparisons of the graph in Fig.24* of inverse Nyquist locis reveals, and there now remains only a small non-minimum phase effect, differences in the slopes of the responses of the two types of columns persist. The effects of changing C (i.e. the vapour/liquid capacitance ratio) was therefore studied next and as Fig. 20 shows, reducing

* Graphs have been normalised for the comparisons.

C makes the slope of the time response of the packed column approach the response of the plate column. Fig 21 again shows time responses of packed and plate columns for a given small C, it is clear that for a small C both columns produce almost identical responses. Effects of changing C was also studied on inverse Nyquist loci of the analytical model defined from P.d.e.'s(47). For C = 1 the model produced satisfactory results as shown in Fig. 6, but unfortunately varying capacitance ratio C in P.d.e.'s (47) does not keep the total capacitance of each section (C+1) constant so that variation in time response slope and locus shape must be expected from this cause. To investigate the effect of capacitance ratio at constant total capacitance, p.d.e.'s(47) and subsequent results need re-expression in terms of $A = 1 - C$

where A = capacitance ratio at constant total capacitance, so P.d.e.'s will change to

$$(1-A) \frac{\partial y}{\partial \tau} - \frac{\partial y}{\partial h} + Gv/V = y_e - y \quad (5.1) \quad (i)$$

$$-(1+A) \frac{\partial y_e}{\partial \tau} - \frac{\partial y_e}{\partial h} + \alpha Gl/V = y_e - y \quad (ii)$$

$$-(1+A) \frac{\partial x'}{\partial \tau} + \frac{\partial x'}{\partial h} + Gl/V = x' - x'_e \quad (iii)$$

$$(1-A) \frac{\partial x'_e}{\partial \tau} + \frac{\partial x'_e}{\partial h} + \alpha Gv/V = x' - x'_e \quad (iv)$$

To find the analytical model same steps as in section (2.4) were taken. Fig. 22 shows inverse Nyquist loci of the packed column for different A, together with the loci of the plate column. It can be seen that reducing A over the frequency of interest makes the response of the packed column to approach the loci of the plate column. Unlike the special case model, the general case model has assumed unequal vapour and liquid capacitances in the column, producing non diagonal (T,F.M.) model even by selecting output and input vectors noted in section (2.4). So unless the (T.F.M.) model is diagonal dominant at a frequency of interest the results are not consistent and can not ignore the interaction terms. Method of Gershgorin circles⁽⁴⁾ has been applied to prove that the (T.F.M.) model is diagonal

dominant at frequency range of 0 to 0.1. Fig.23 shows the loci of the packed column for a small A with Gershgorin circles on it. It is clear that up to $\omega = 0.1$ none of the circles, encircle the origin, so (T.F.M.) is diagonal dominant up to $\omega = 0.1$.

6. Discussions and conclusions

A parametric analytical (T.F.M.) model has been derived for an asymmetrical binary distillation columns, where all the parameters are expressed as functions of plant parameters, α, C, L, T . As it is noted in sections (2) the model has been derived in terms of normalised distance h and normalised frequency P . In order to convert h to actual distance must multiply it by V/K and also to convert normalised time to actual, multiply it by H/K . All symbols are explained in list of symbols. The derivations of the general case model⁺ did not produce a completely diagonal (T.F.M.) at all frequencies as it was the case for the special case (equal vapour liquid capacitances model, but the general case model⁺ was found to be diagonal dominant at low frequencies.

Use of inverted U tube to represent the distillation column has helped greatly the solutions, specially for terminal composition changes.

In packed columns g_2 has negative gain at low and high frequencies, this is the case for plate columns too. g_1 in shorter packed columns has negative gain at low and high frequencies, but for relatively longer packed columns g_1 has positive gain at low frequencies and negative gain at high frequencies producing a non-minimum phase effect. In plate type columns g_1 has always positive gain.

Large terminal capacitance, effects only the calibration of the low frequency part of the inverse Nyquist loci, therefore it effects the initial rate of rise of the transient responses.

Wave effects in longer packed columns may be neglected, but non-minimum phase effects can cause limitations in choosing the maximum controller gain in order to achieve stable operations.

+ unequal vapour and liquid capacitances

In long packed columns as columns' vapour capacitance becomes smaller the behaviour of packed and plate columns become closer to one another in both time and frequency domain. (Although a small residual non-minimum phase effect is present with packed type columns even for large L.) It was originally anticipated that c (i.e. the vapour/liquid capacitance ratio) alone would be the key parameter in reconciling the behaviour of the two column types, but it has become evident that L and c together are crucial.

References

1. EDWARDS, J.B.: 'The analytical modelling and dynamic behaviour of a spatially continuous binary distillation column'. Research Report
2. EDWARDS, J.B.: 'The analytical modelling and dynamic behaviour of tray-type binary distillation columns'. Research Report
3. EDWARDS, J.B. and OWENS, D.H.: 'First order type models for multi-variable process control'. Proc. I.E.E., 1977, 124(11), pp. 1083-1088.
4. ROSENBROCK, H.H.: 'Computer-aided control systems design'.
5. GUILANDOUST, M. 'Progress in the Dynamic Analysis of Symmetrical Packed Distillation Column', Research Report No. 107, January 1980.

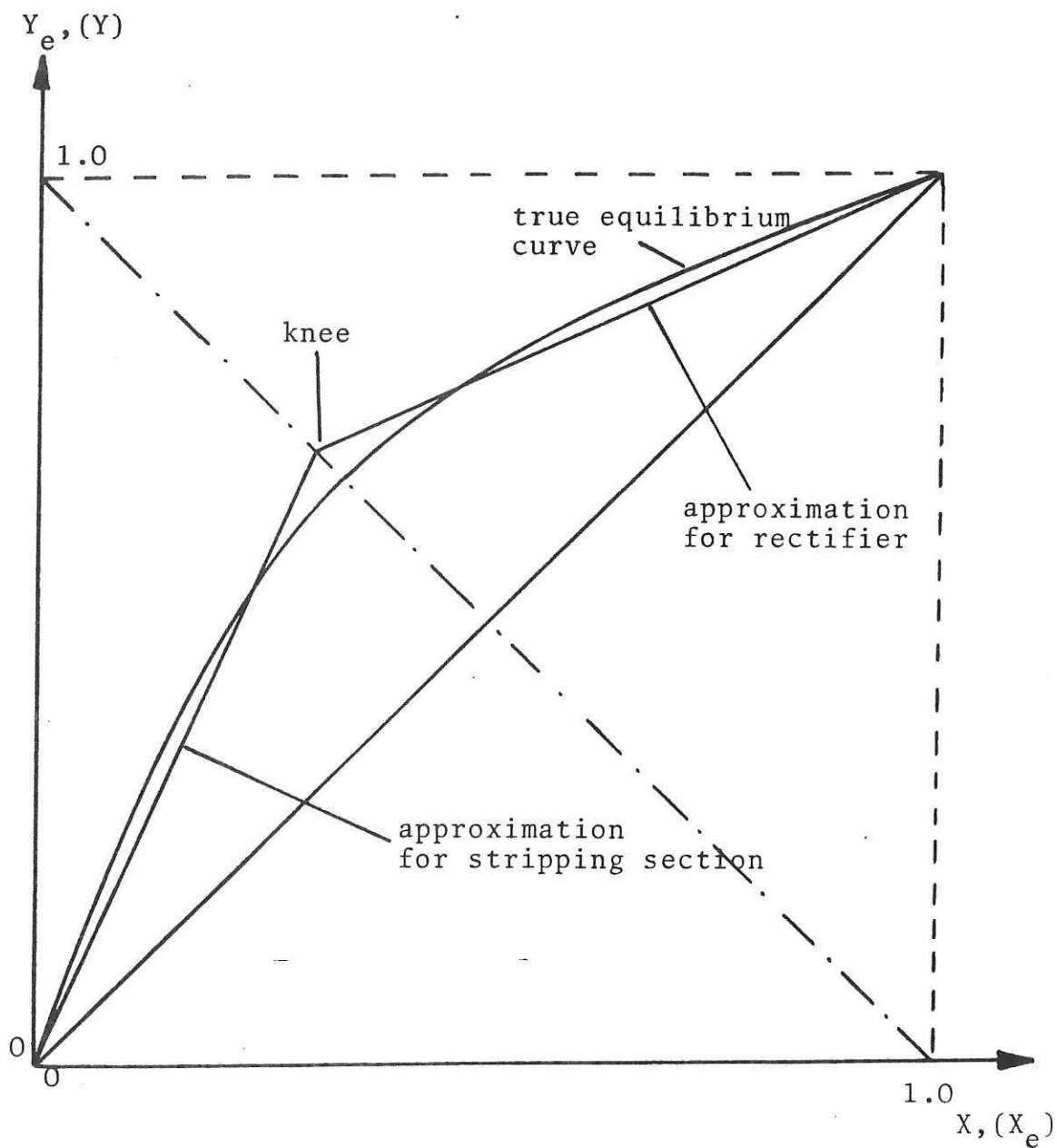


Fig. 1. Ideal equilibrium curve for binary mixture and its piecewise-linear approximation

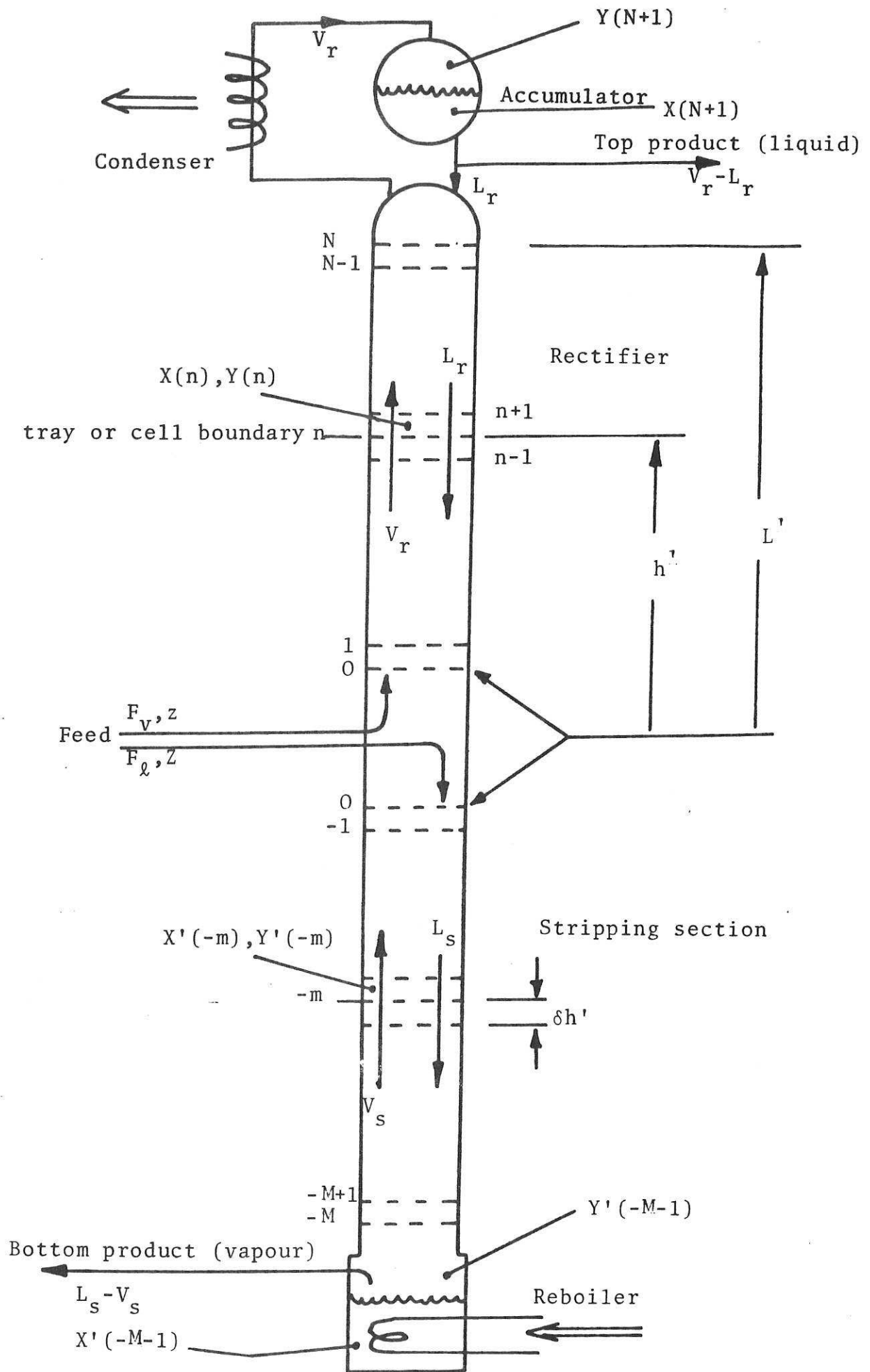


Fig. 2. General arrangement of binary distillation column

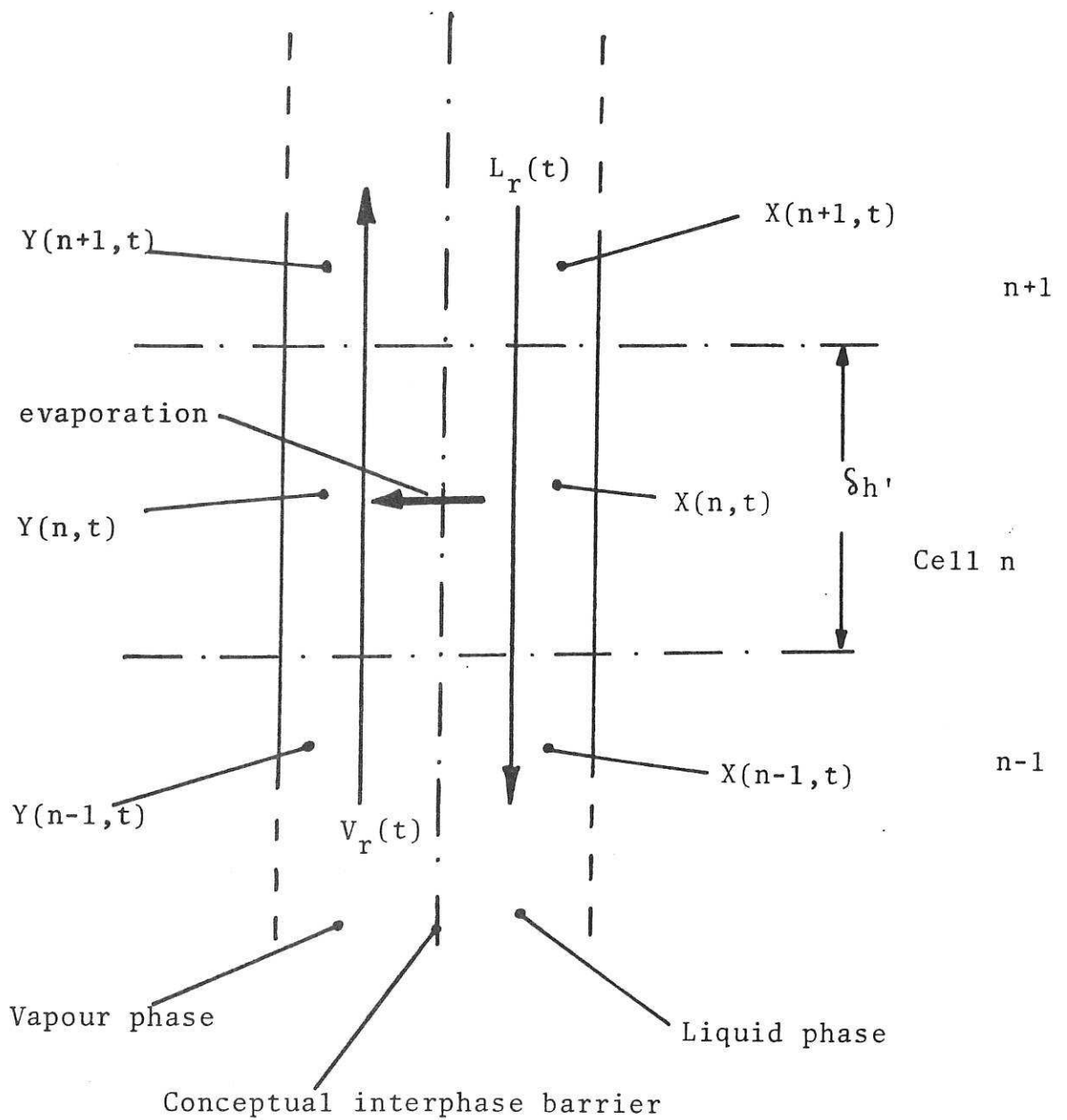


Fig. 3 Variables associated with n'th cell of column rectifying section.

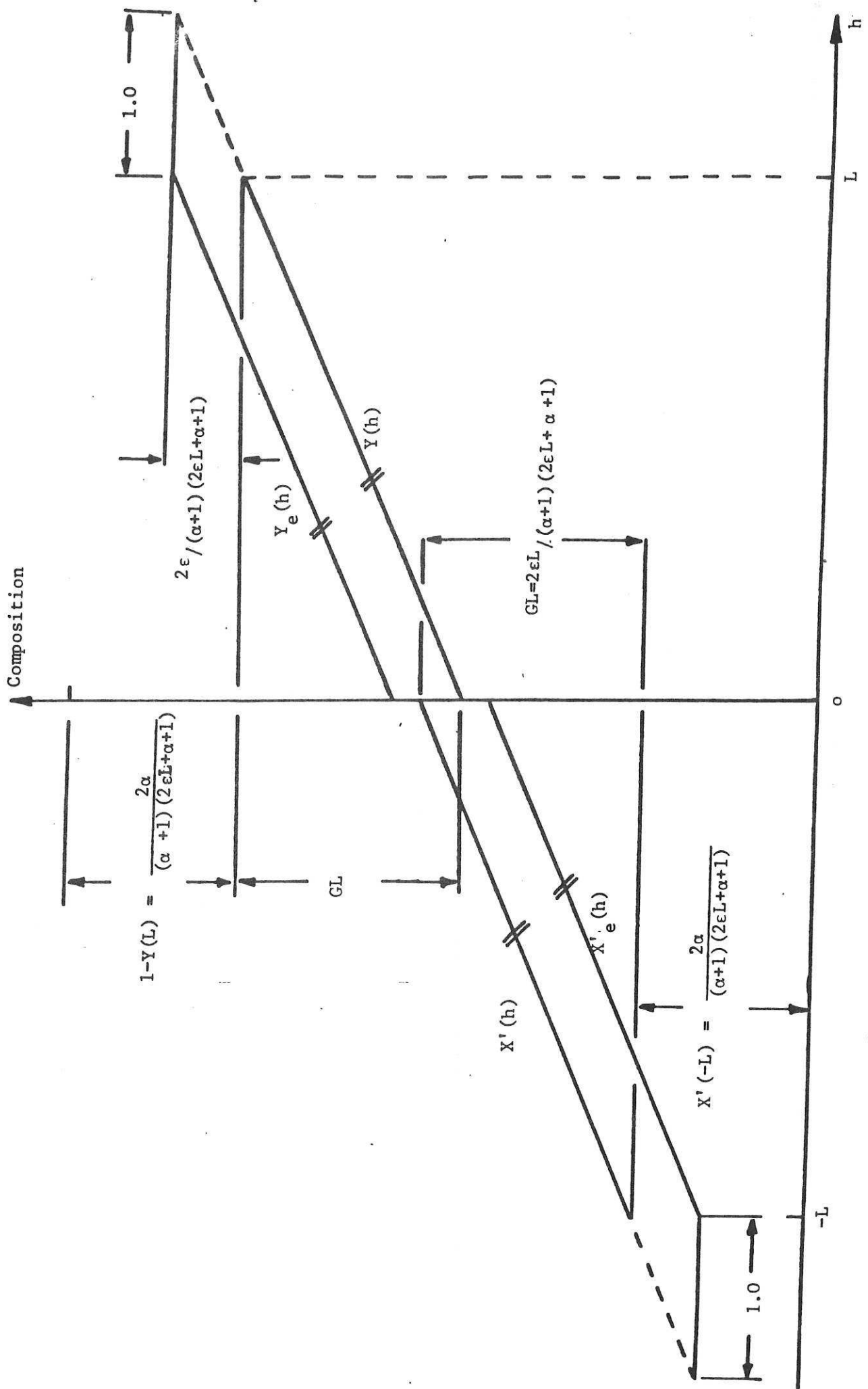


Fig. 4. Steady-state composition profiles

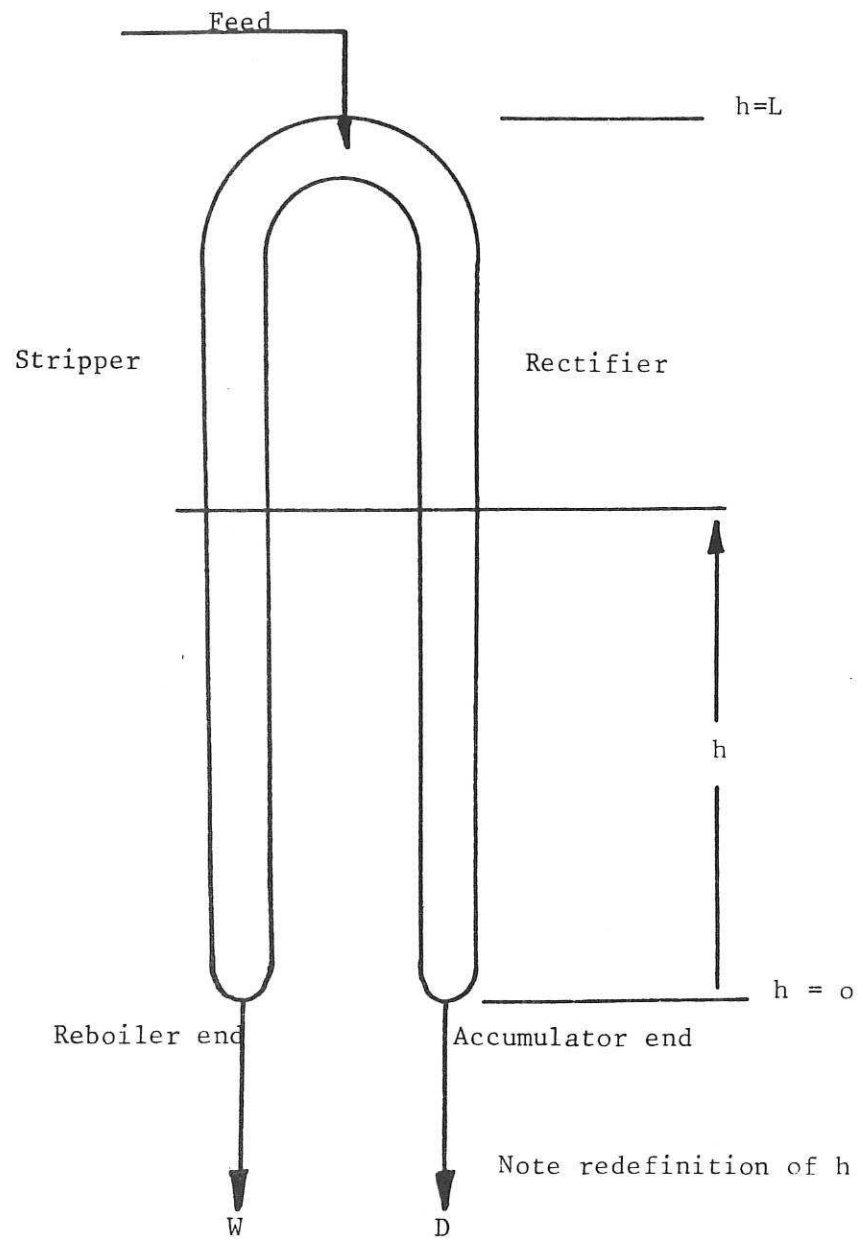


Fig. 5 Inverted U-tube model

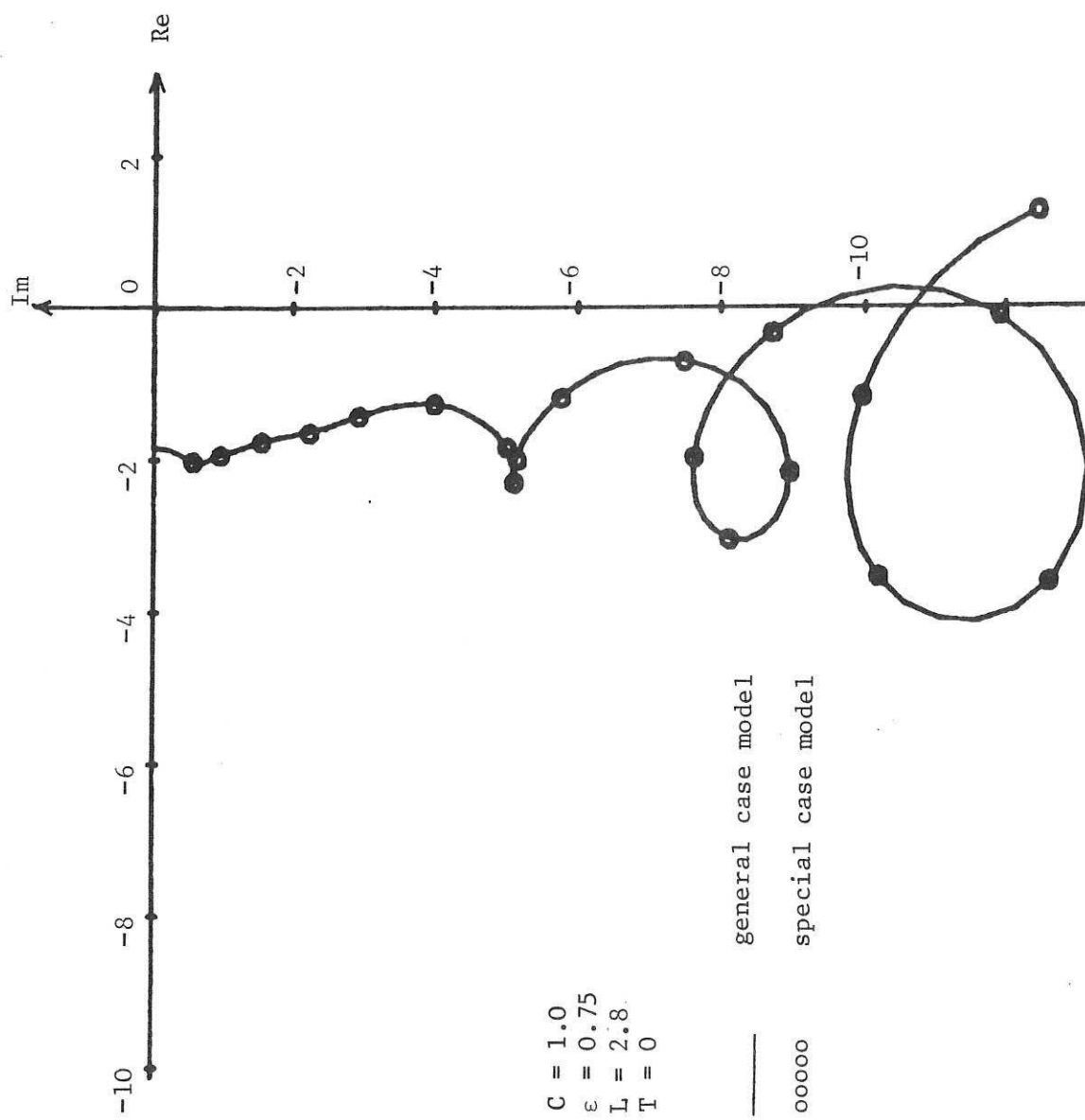


Fig. 6. Loci of $g_1^{-1}(0, j\omega)$ for the packed columns

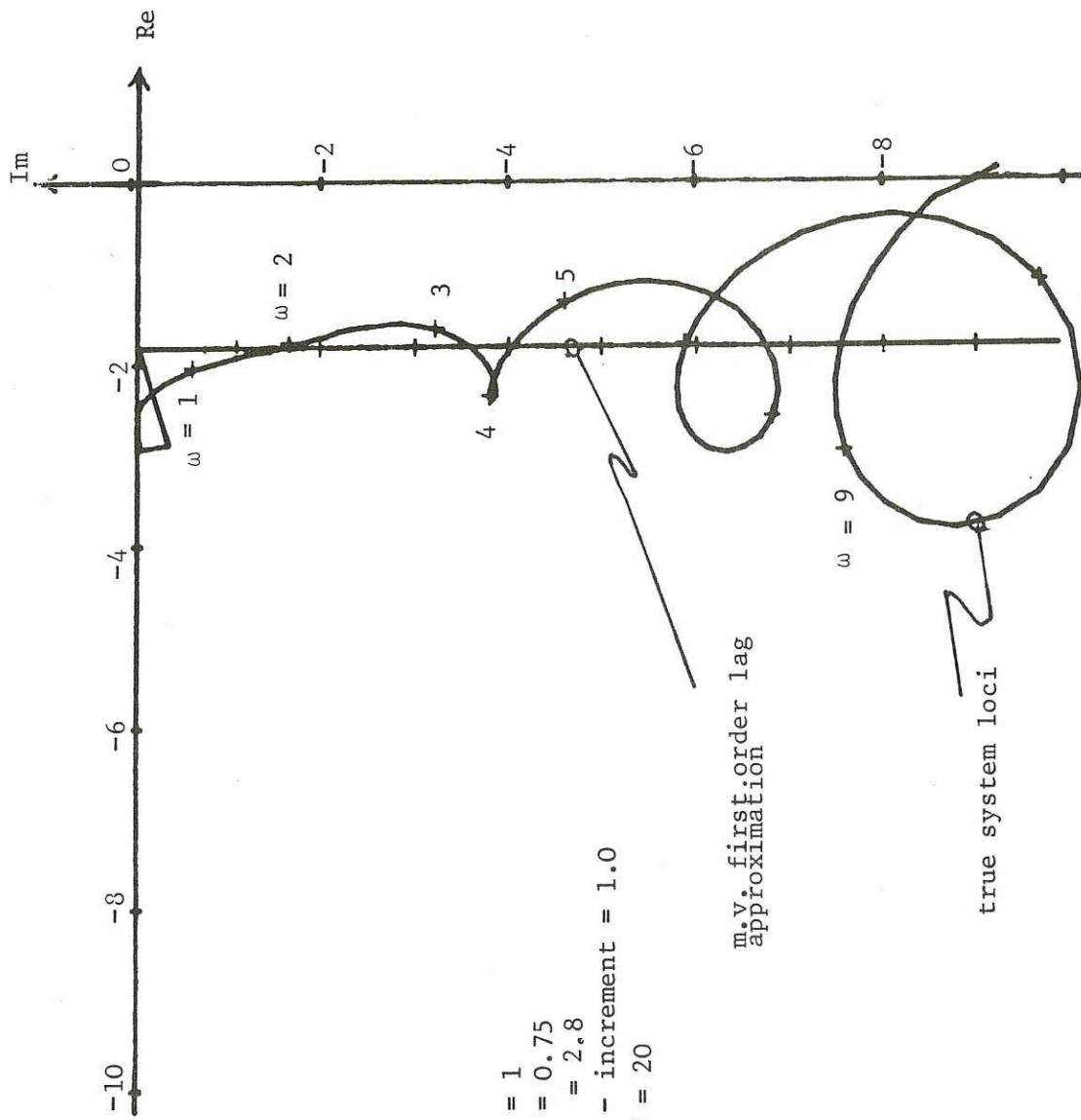


Fig. 7. Loci of $g_1^{-1}(0, j\omega)$ for packed columns with its multivariable

first order lag approximations

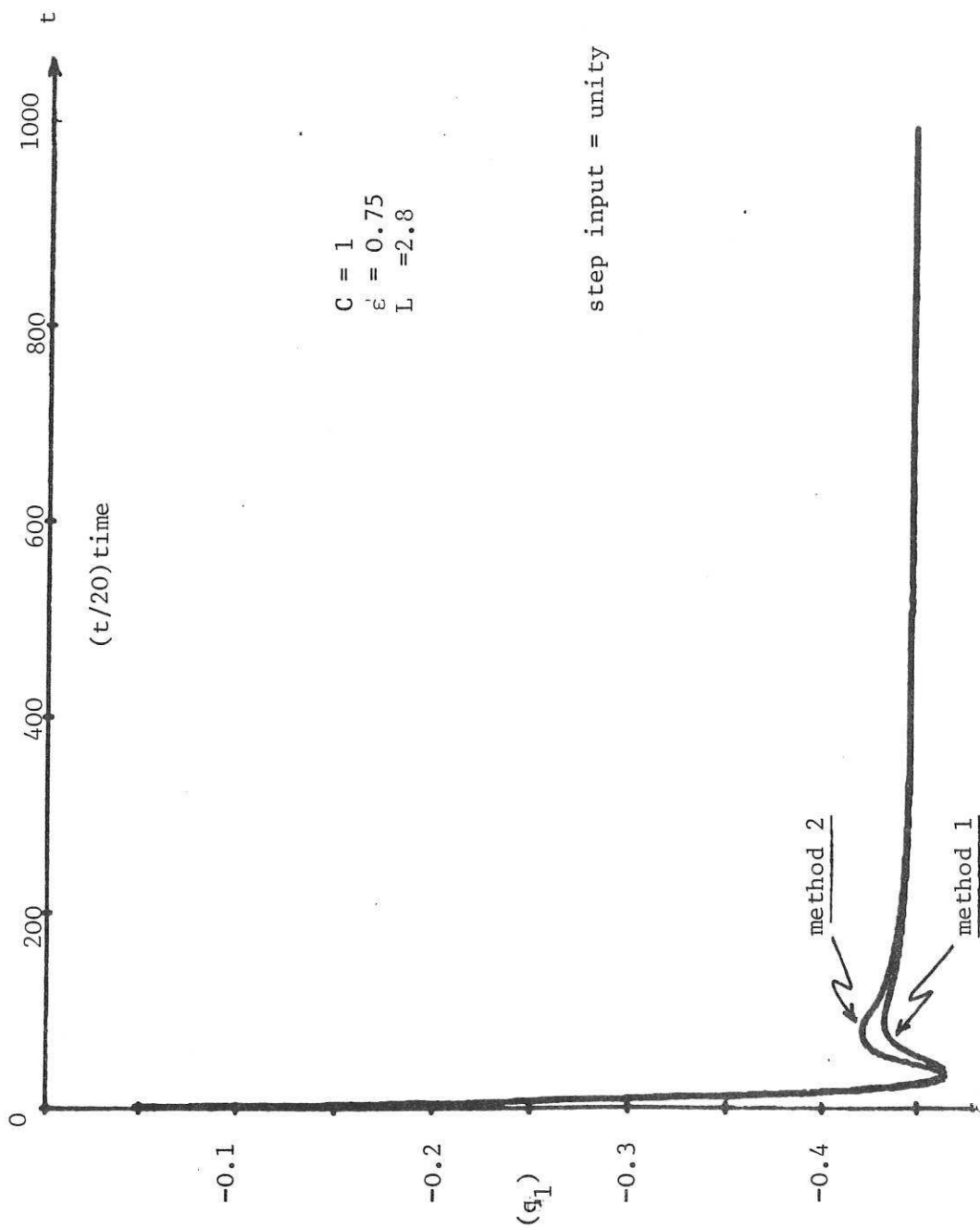


Fig. 8. Time responses of q_1 for the packed columns by the two methods of updating of the multi pass theory

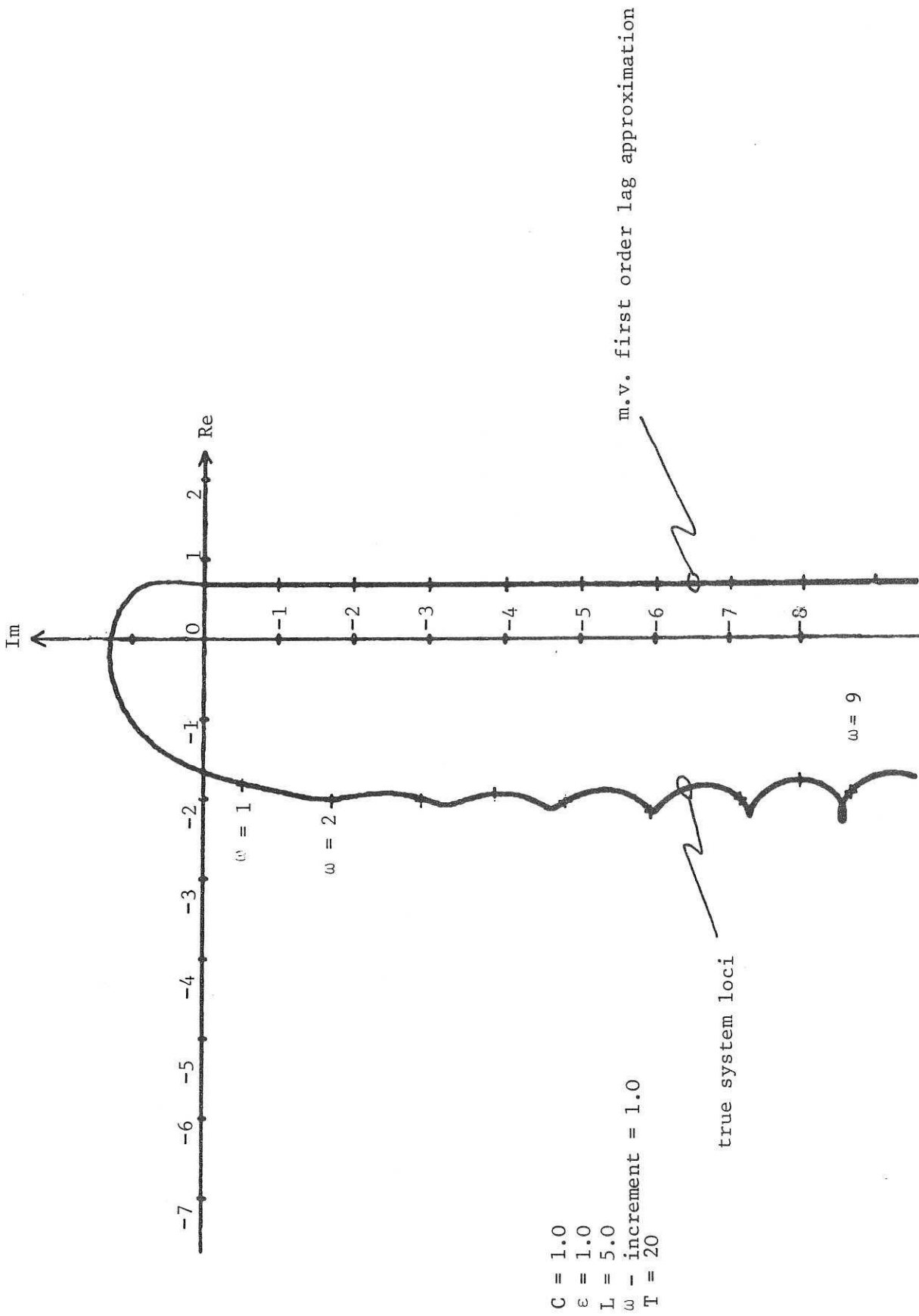


Fig. 9. Loci of $g_1^{-1}(0, j\omega)$ for packed columns

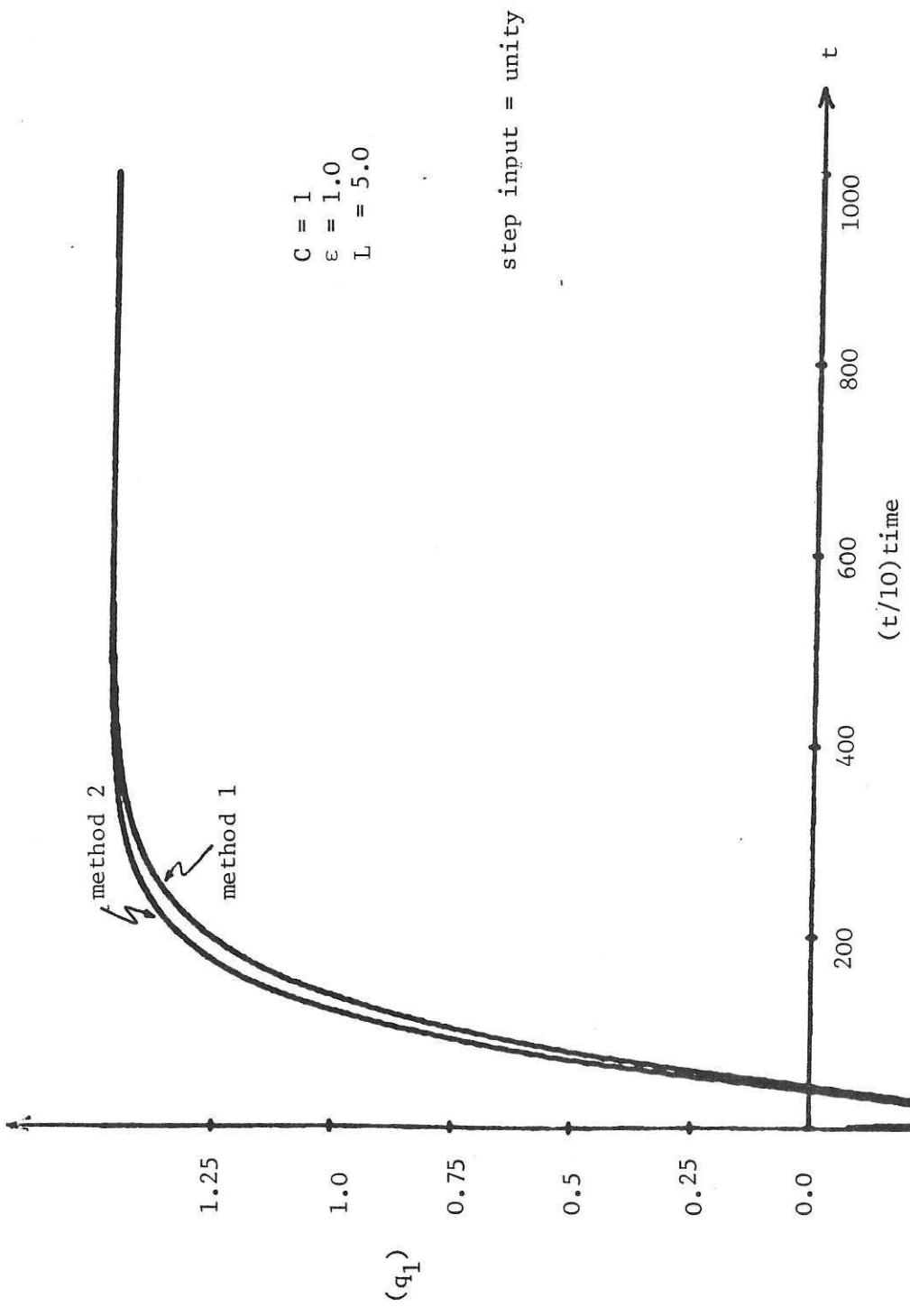


Fig. 10 Time response of q_1 for the packed columns

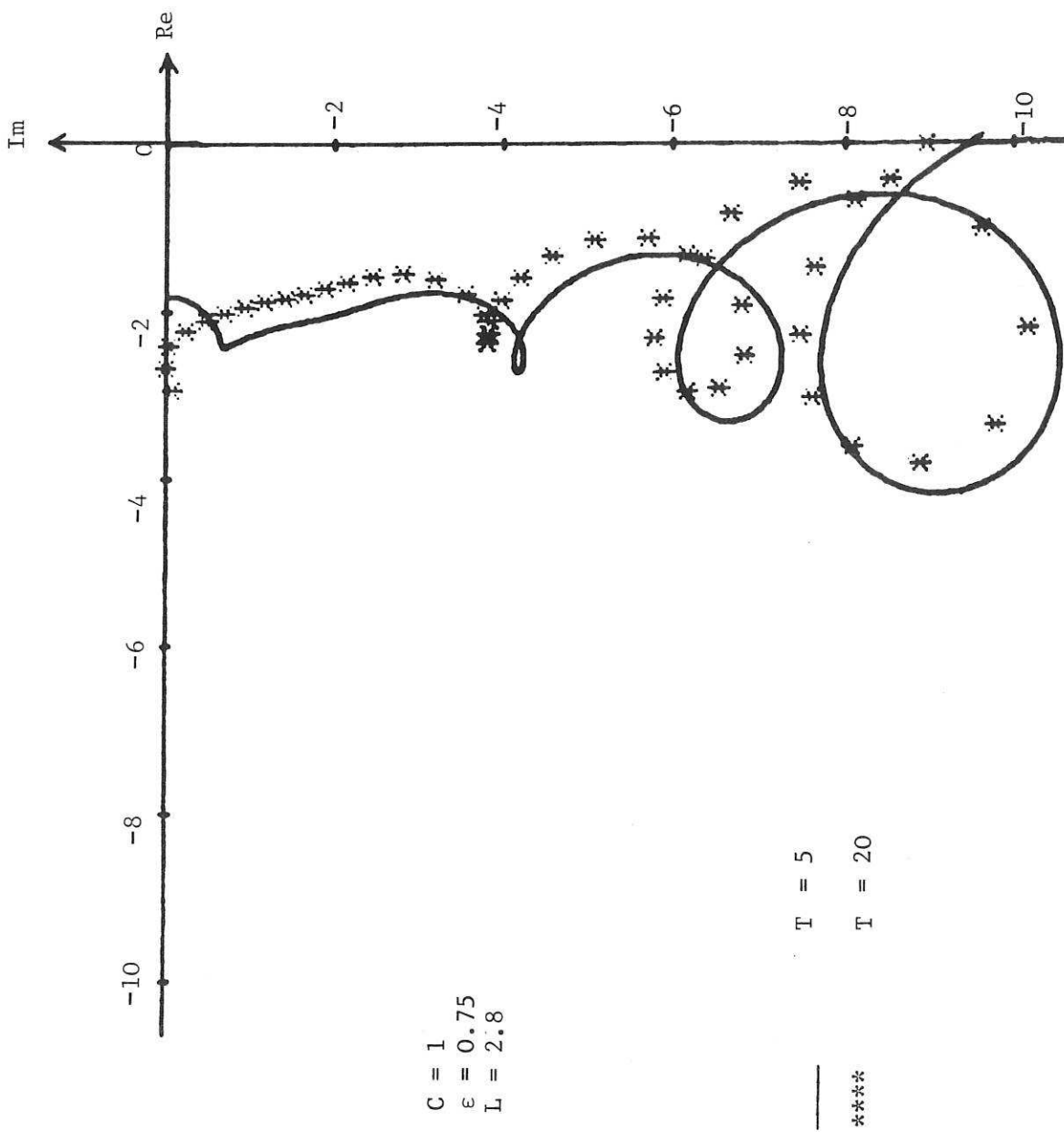


Fig. 11 Loci of $g^{-1}(0, j\omega)$ for the packed column

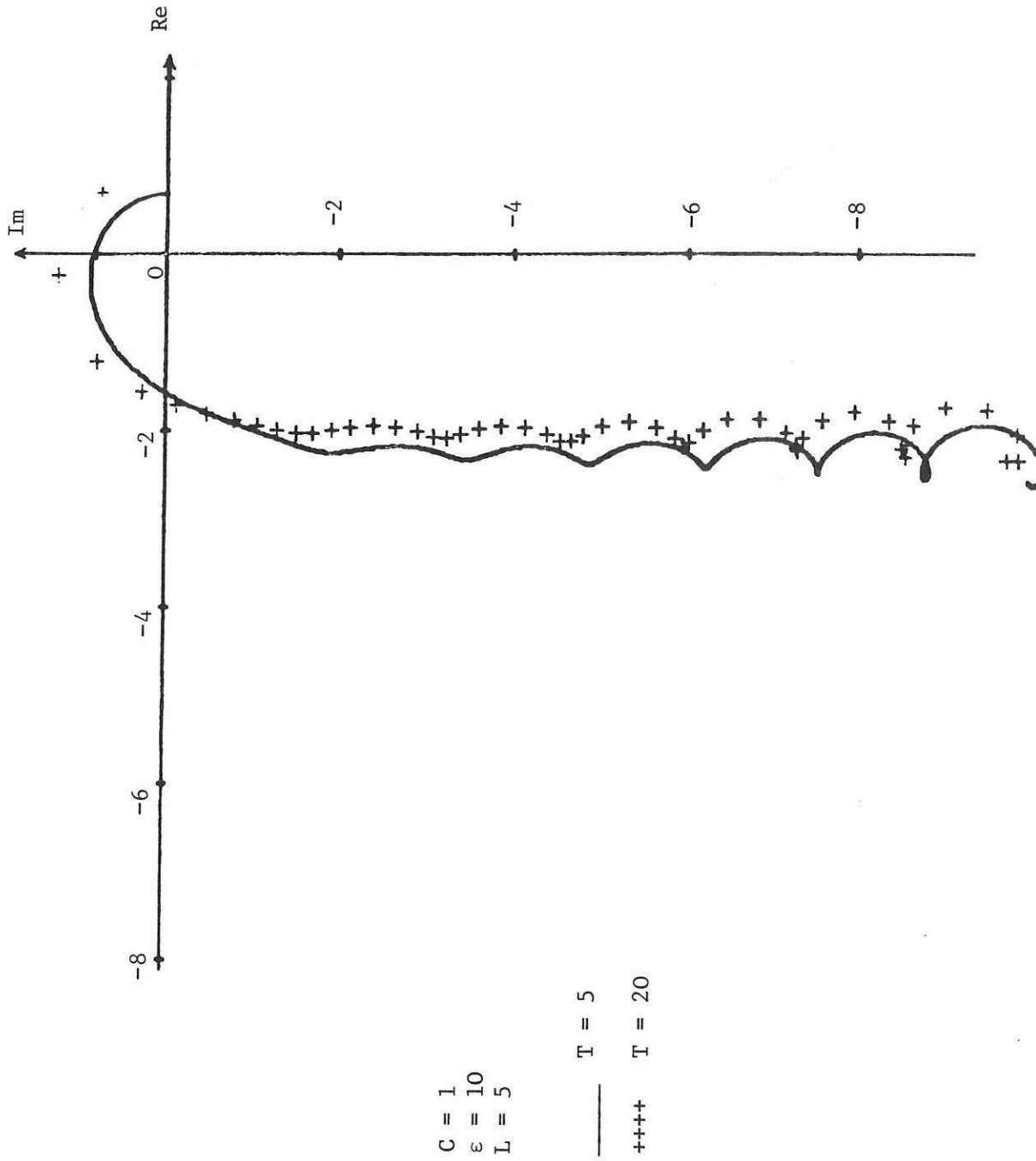


Fig. 12 Loci of the $g^{-1}(0, j\omega)$ for the packed column

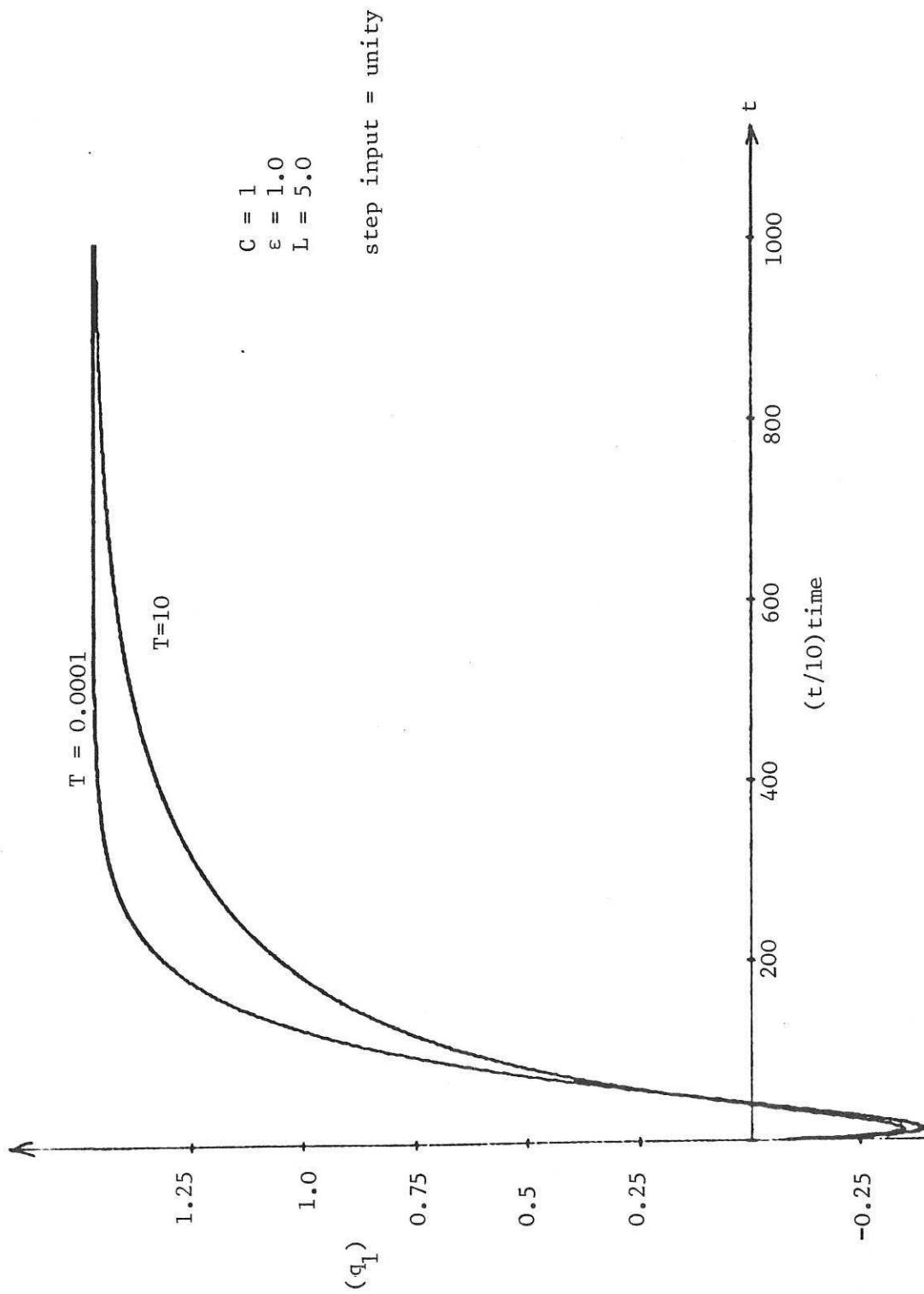


Fig. 13 Time response of q_1 for the packed column.

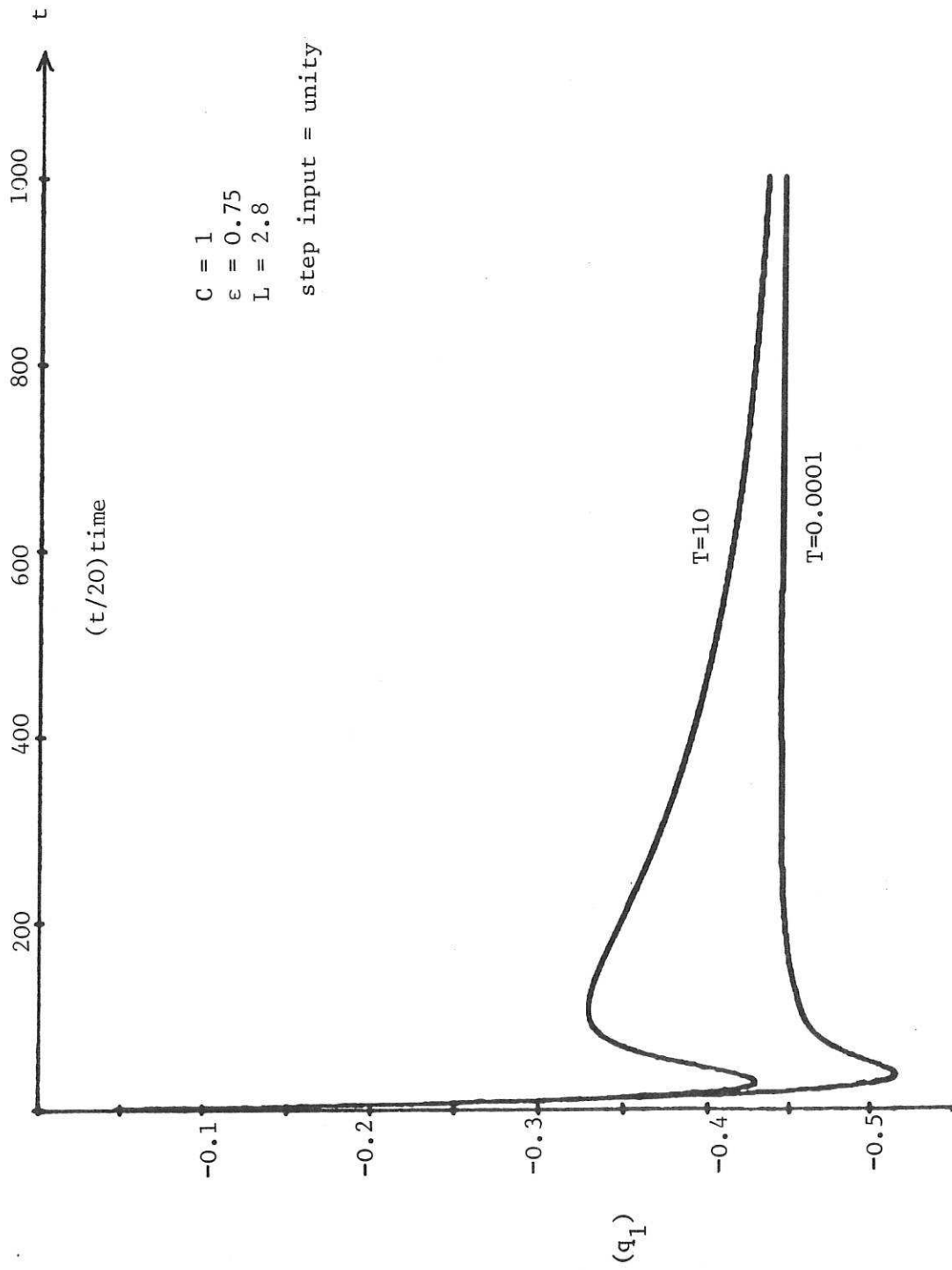


Fig. 14 Time response of q_1 for the packed column

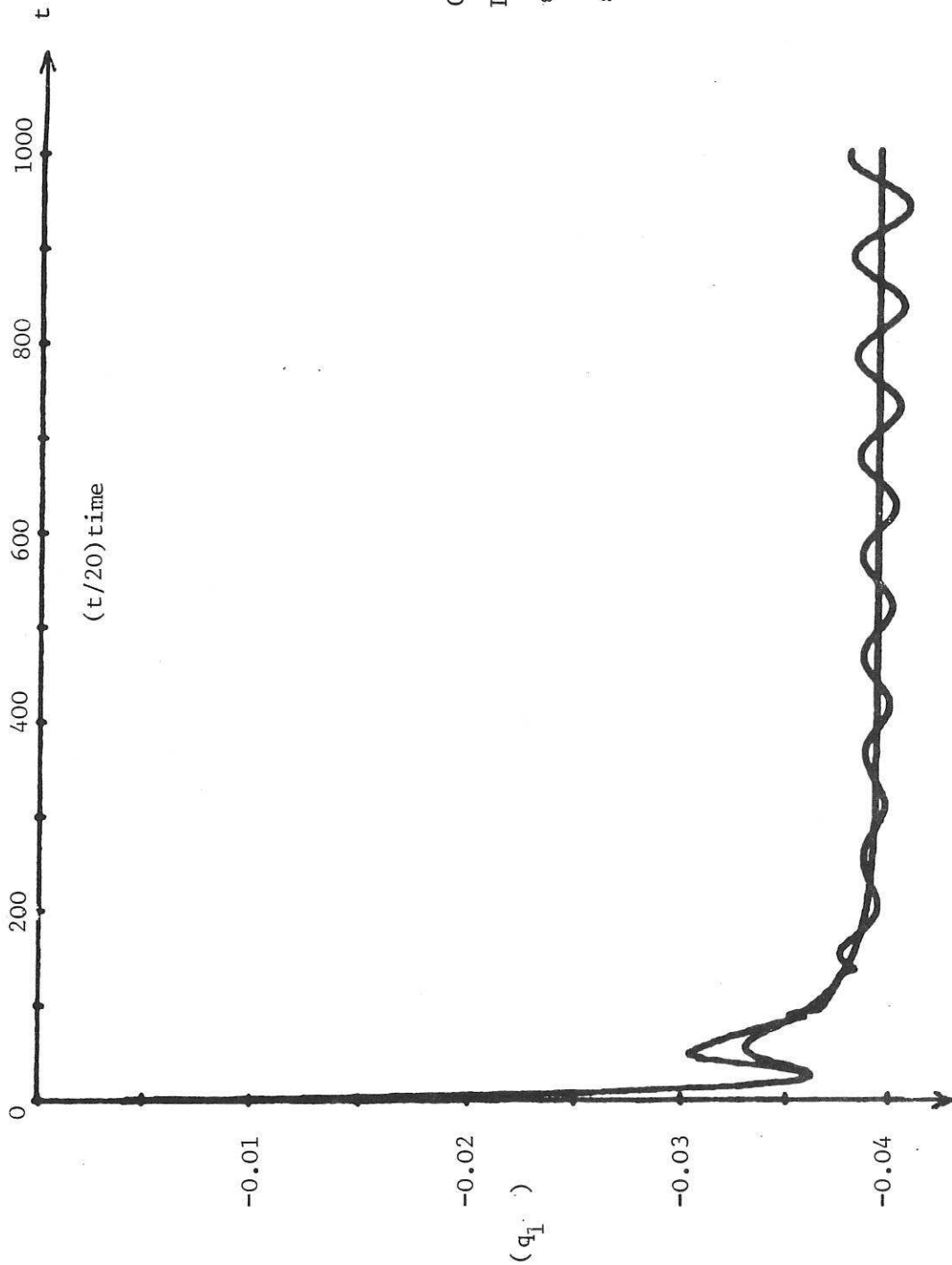


Fig 15 Time response of (q_I) for the packed columns by the two methods of updating for the multi pass analyses

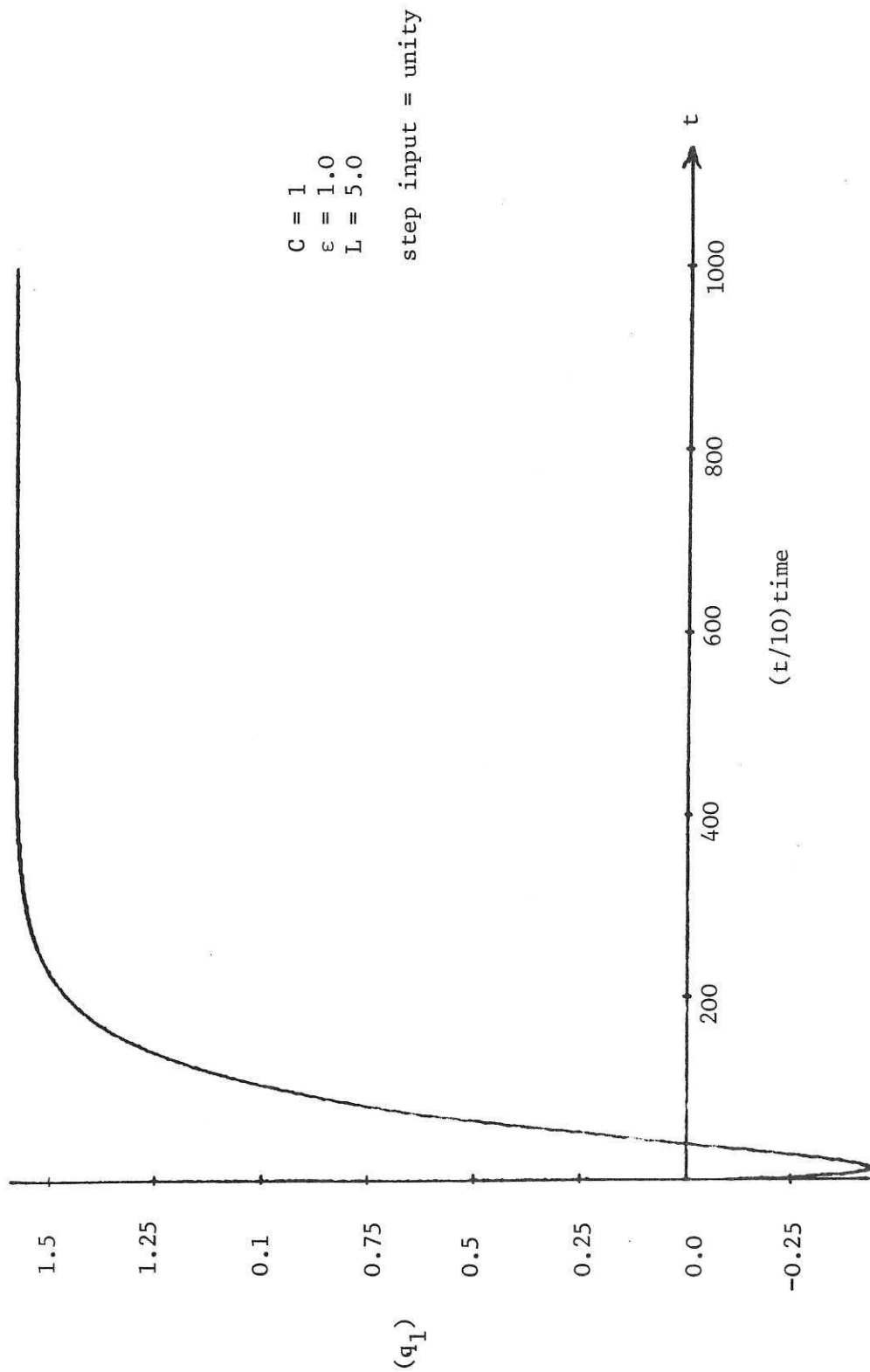


Fig. 16 Time response of q_1 for the packed column

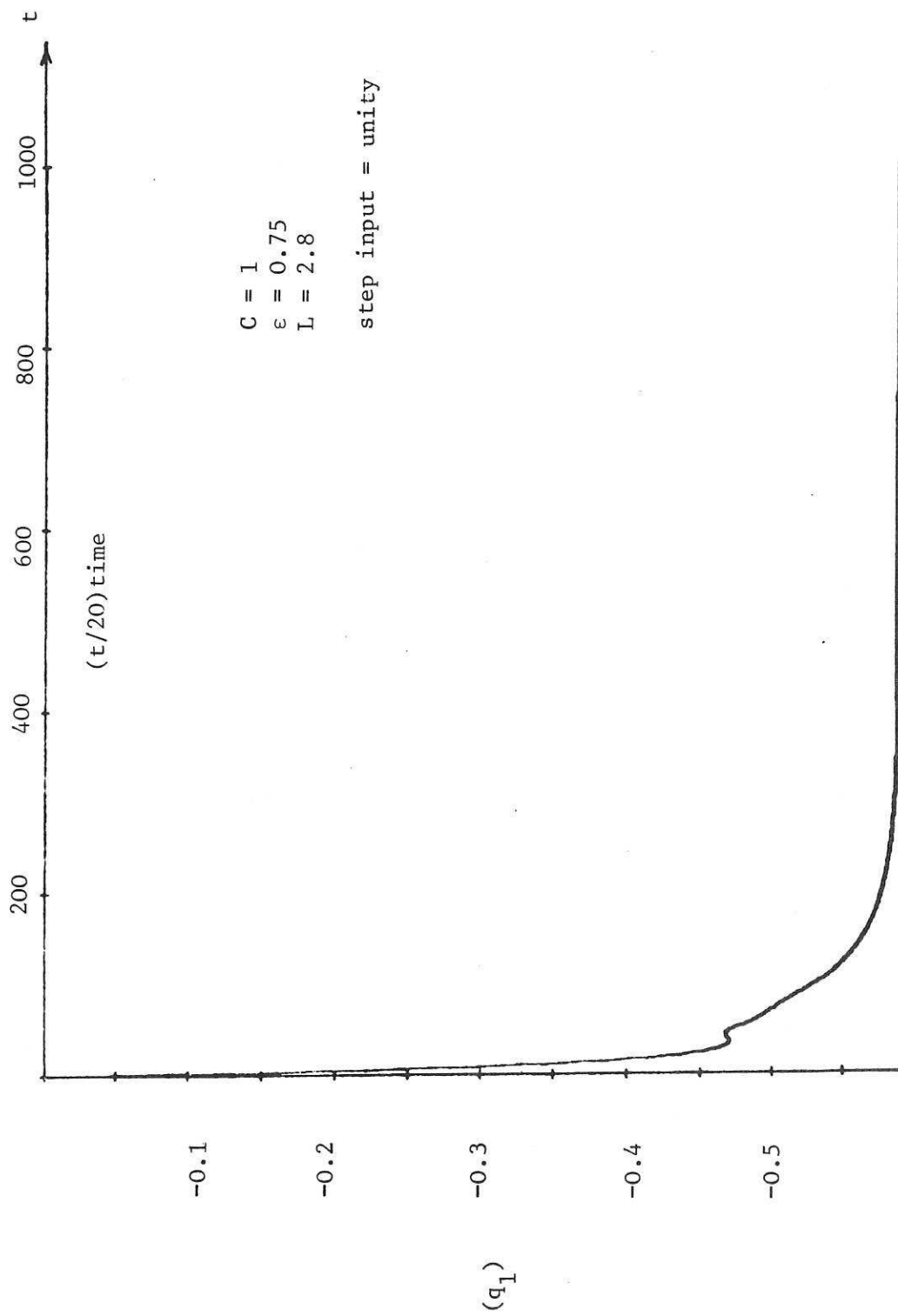


Fig. 17 Time response of q_1 for the packed column

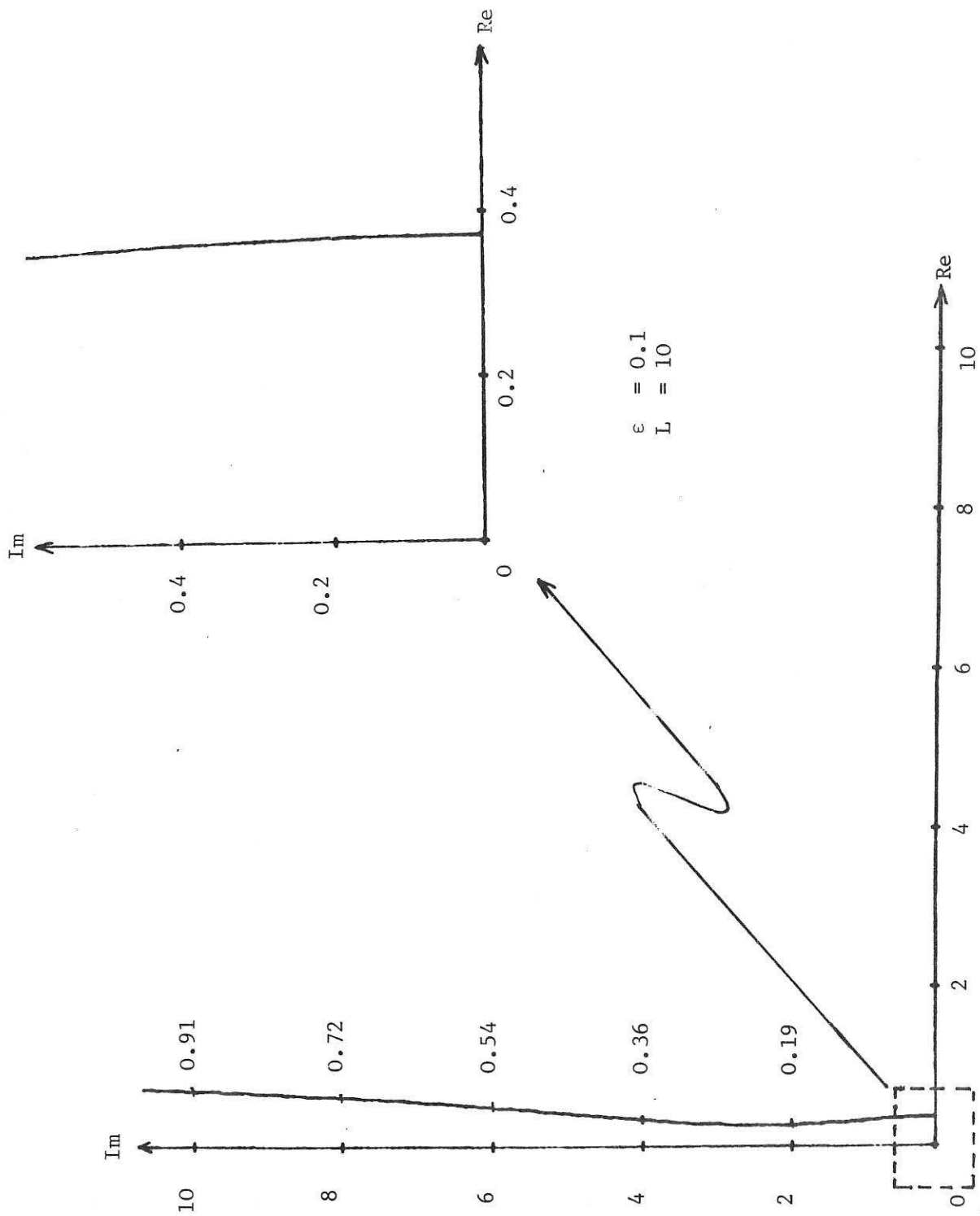


Fig. 18 Inverse Nyquist Loci of $g_1^{-1}(0, j\omega)$ for the plate column

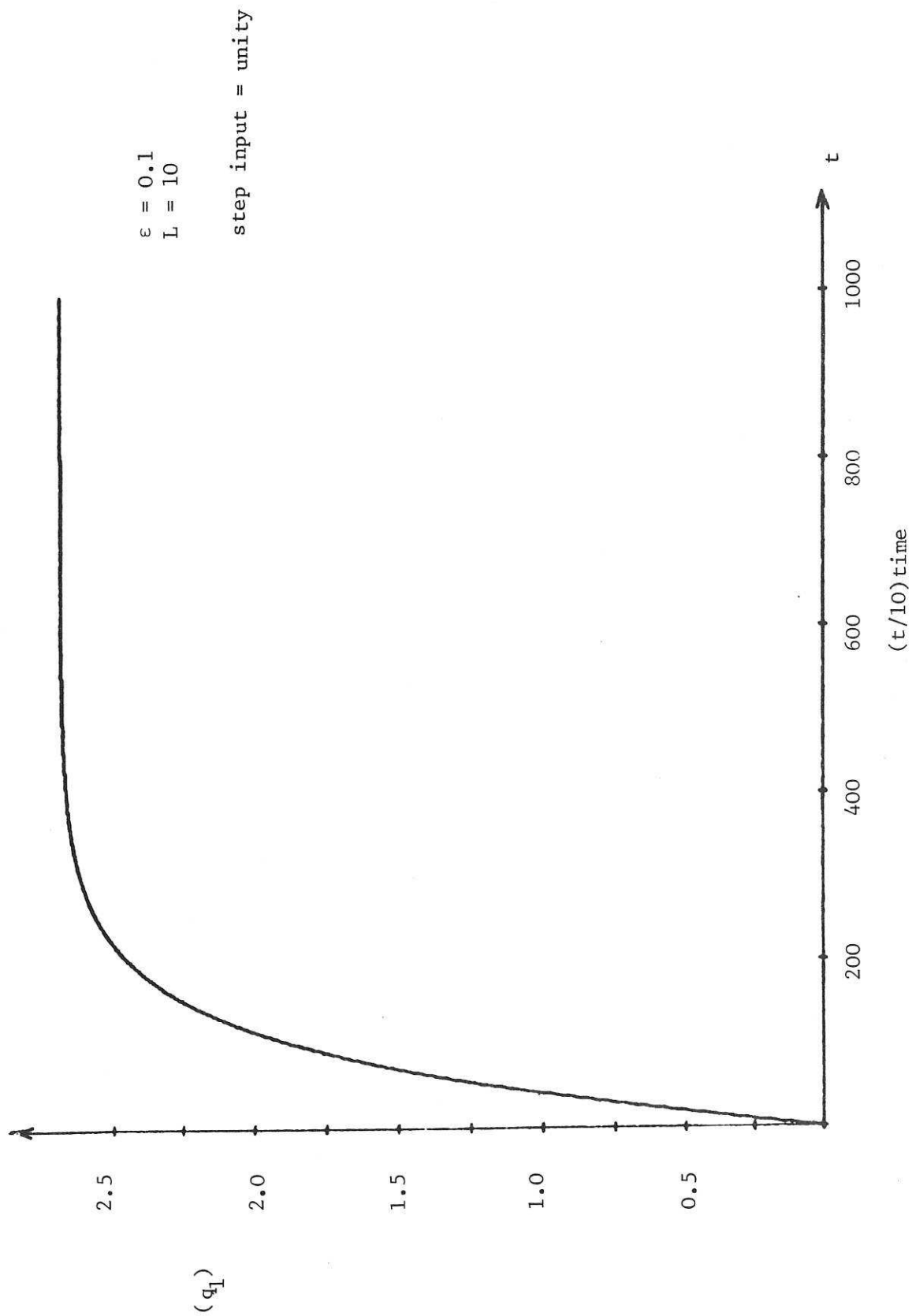


Fig. 19. Time response of q_1 for the plate column

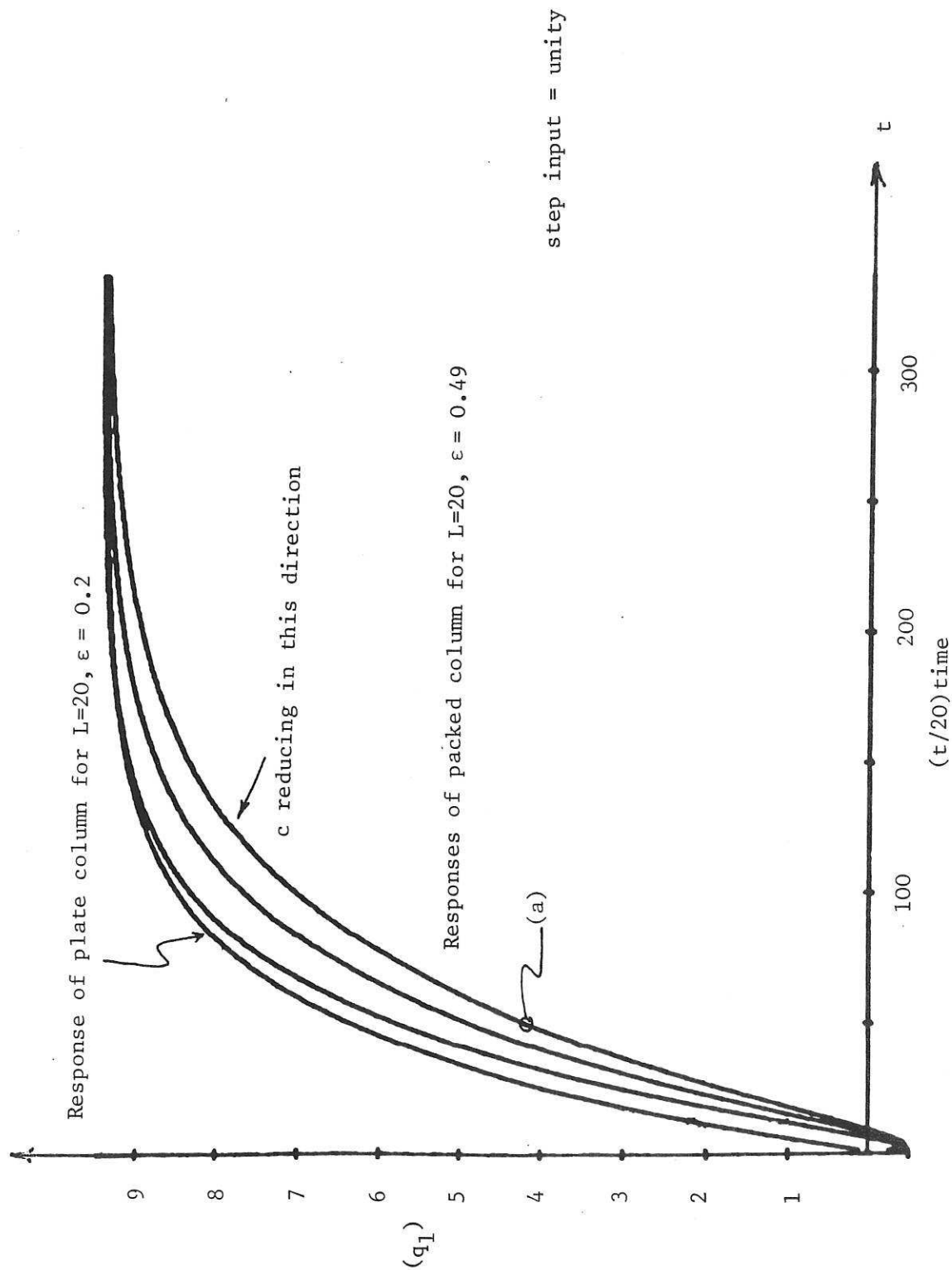


Fig. 20 Effect of changing c for the packed column and comparing with that of the plate column.

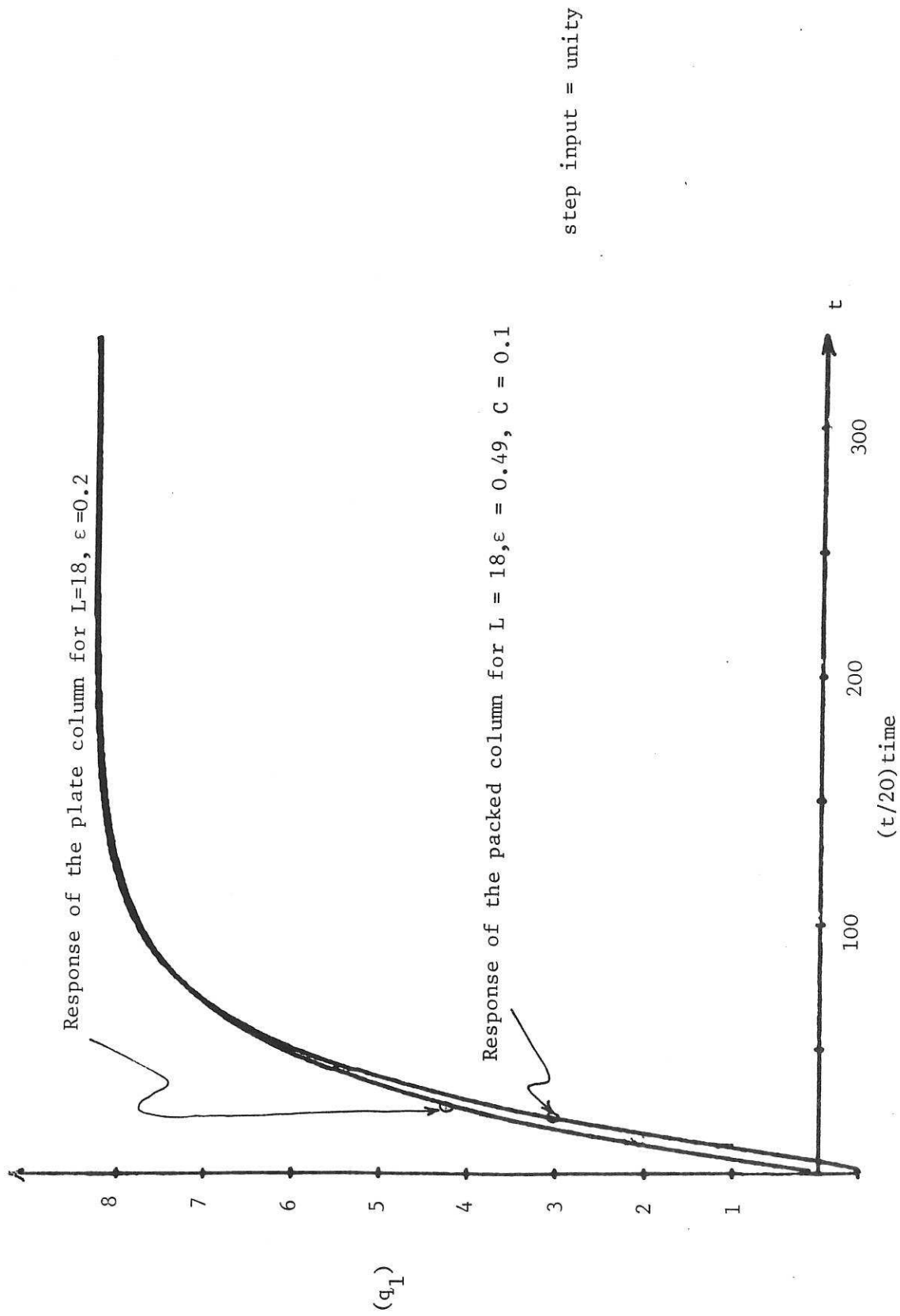


Fig. 21 Response of the packed column together with the response of plate column

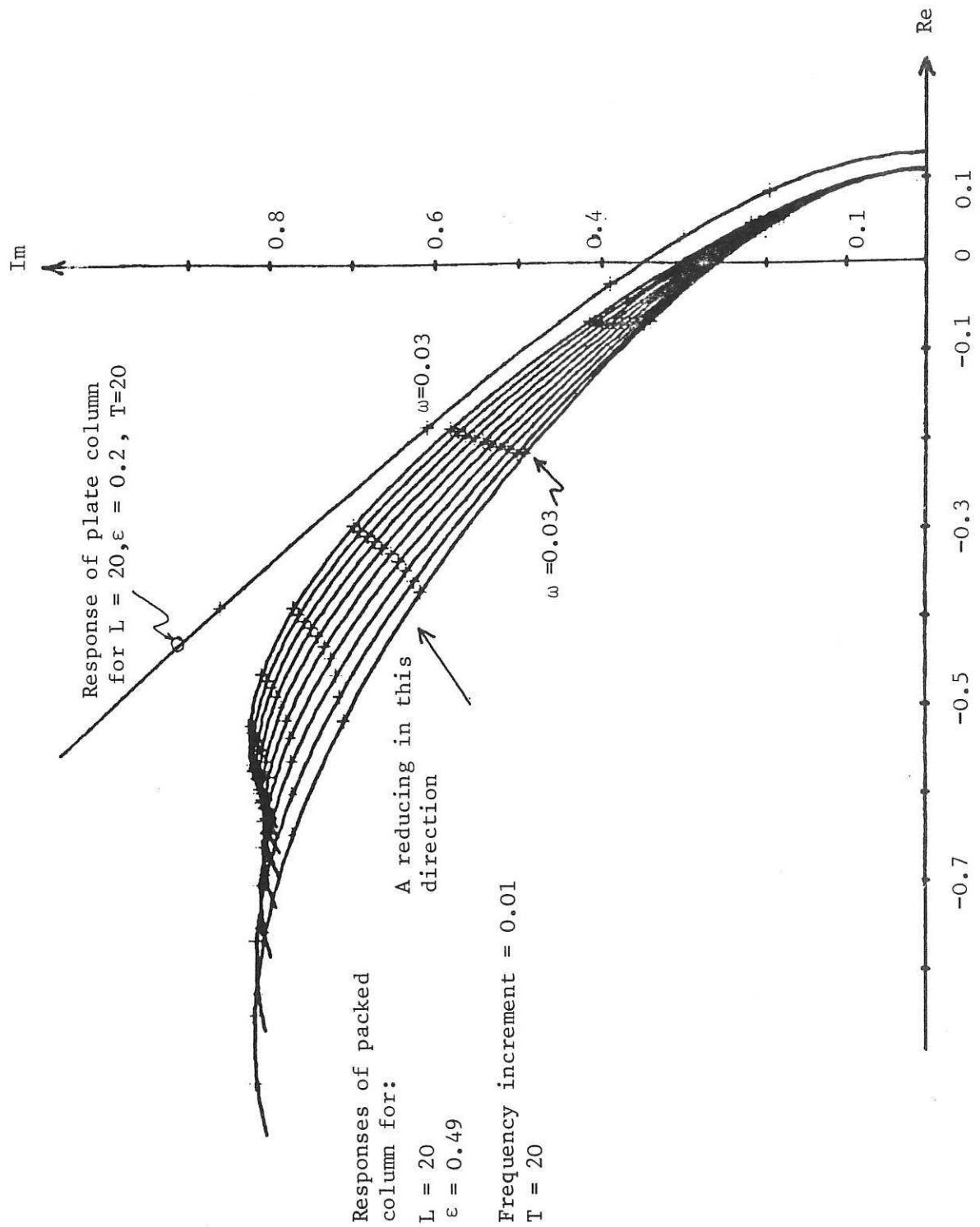


Fig. 22 Inverse Nyquist loci of $g(0, j\omega)^{-1}$ for packed and plate columns and effect of changing C

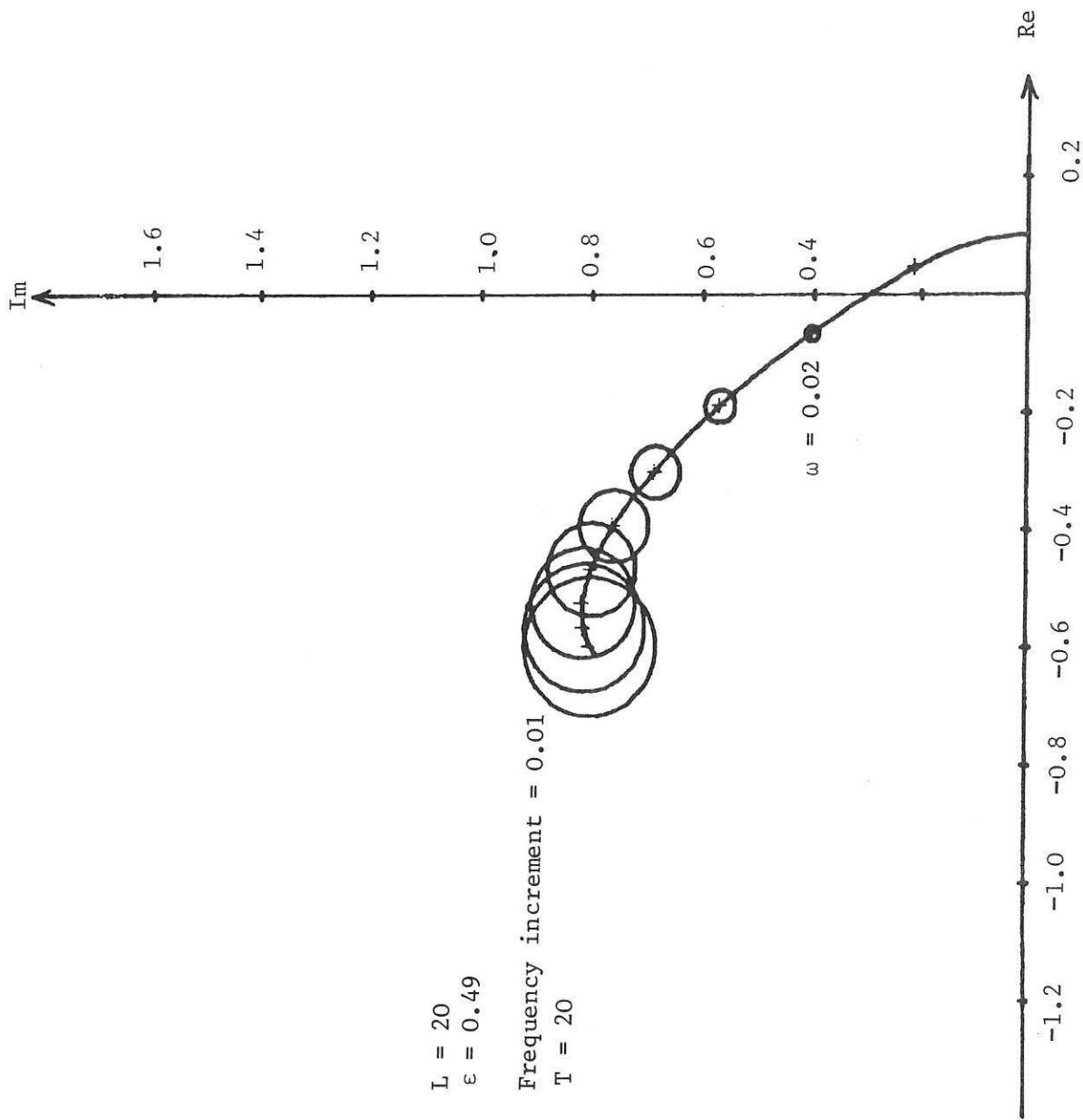
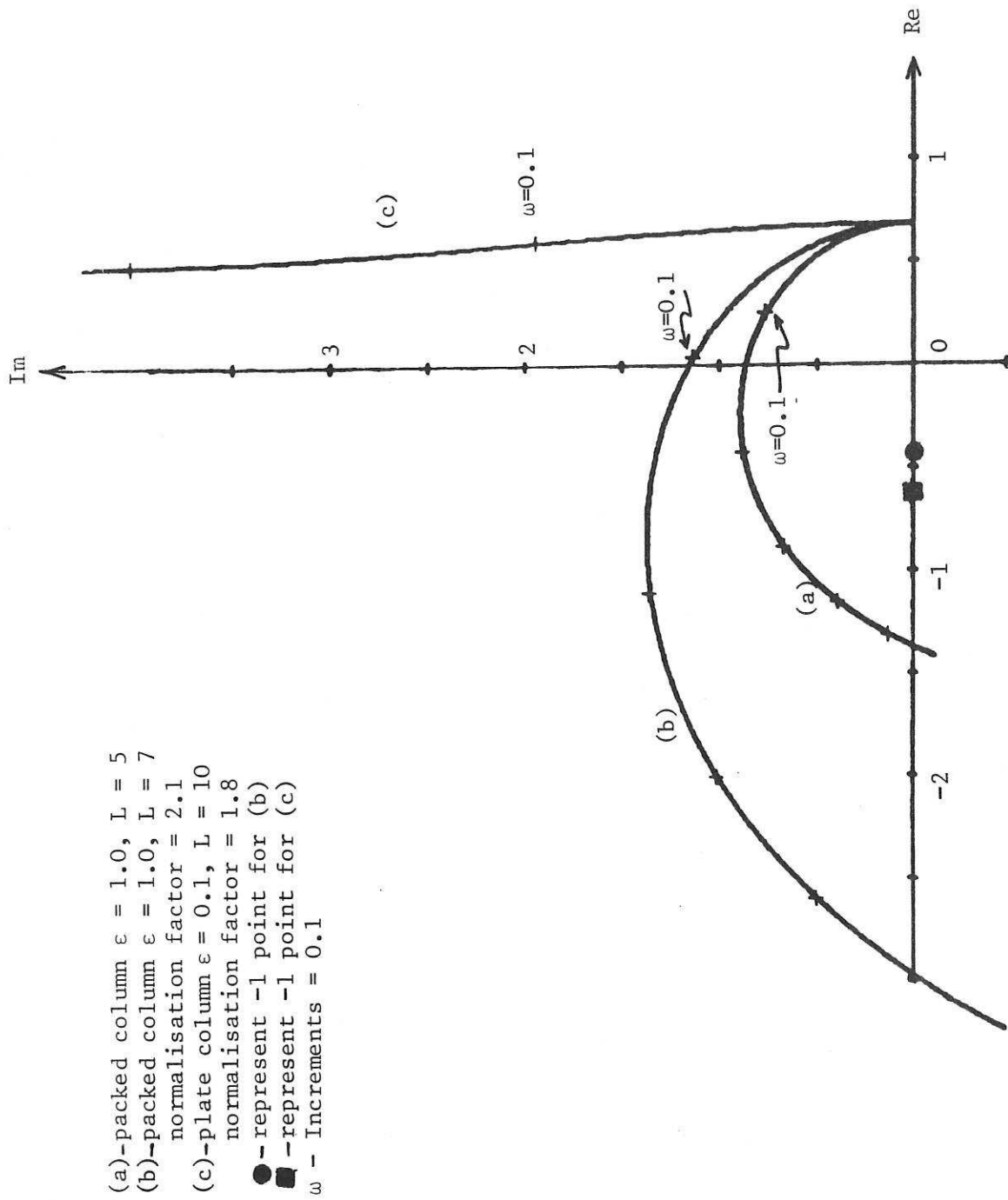


Fig. 23 Inverse Nyquist Loci of $g^{-1}(0, j\omega)$ for packed column of small A and Gershgorin circles on it.



- (a)-packed column $\epsilon = 1.0, L = 5$
- (b)-packed column $\epsilon = 1.0, L = 7$
normalisation factor = 2.1
- (c)-plate column $\epsilon = 0.1, L = 10$
normalisation factor = 1.8
- - represent -1 point for (b)
- - represent -1 point for (c)
- ω - Increments = 0.1

Fig. 24. Inverse Nyquist Locus for the packed and plate columns